JGR Solid Earth

RESEARCH ARTICLE
10.1029/2023JB027766

Thermal Stressing of Volcanic Rock: Microcracking and Crack Closure Monitored Through Acoustic Emission, Ultrasonic Velocity, and Thermal Expansion

L. Griffiths[1,2], M. J. Heap[2,3], O. Lengliné[2], P. Baud[2], J. Schmittbuhl[2], and H. A. Gilg[4]

[1]NGI—Norwegian Geotechnical Institute, Oslo, Norway, [2]UMR 7063, CNRS, Institut Terre et Environnement de Strasbourg, Université de Strasbourg, Strasbourg, France, [3]Institut Universitaire de France (IUF), Paris, France, [4]Department of Civil, Geo and Environmental Engineering, Technical University of Munich, Munich, Germany

Abstract Microcracking due to thermal stresses affects the mechanical and flow properties of rocks, which is significant for thermally dynamic environments such as volcanoes and geothermal reservoirs. Compared with other crustal rocks like granite, volcanic rocks have a complex and variable response to temperature; it remains unclear how thermal microcracks form and how they are affected by temperature. We heated and cooled samples of low-porosity basalts containing different amounts of microcracks and a porous andesite over three cycles, whilst monitoring microstructural changes by acoustic emission (AE) monitoring and measurement of *P*-wave velocity (v_P; up to 450°C) and thermal expansion coefficient (TEC; up to 700°C). During the second and third cycles, the TEC was positive throughout and the rate of detected AE was low. In contrast to studies on granite, we measured a strong and reversible increase in v_P with increasing temperature (by 15%–40% at 450°C), which we interpret as due to microcrack closure. During the first cycle, AE and v_P measurements indicated thermal microcracking within the andesite and the basalt with a low initial microcrack density. For these samples, strong inflexions in the TEC indicated stress relaxation during heating, preceding significant thermal microcracking during cooling. The basalt with a high initial microcrack density underwent little microcracking throughout all cycles. Our results and a review of the literature relate the initial microstructure to the occurrence of thermal microcracking and explore the potentially significant influence of temperature on volcanic rock properties.

Plain Language Summary Microcracking due to thermal stresses affects the mechanical and flow properties of rocks, playing an important role within volcanoes and geothermal reservoirs. Volcanic rocks exhibit a complex response to temperature, and it remains unclear how thermal microcracks form and how they are affected by temperature. Here, we repeatedly heated and cooled samples of basalt and andesite with different initial porosities and microcrack content over three heating/cooling cycles, whilst monitoring for laboratory-scale seismicity and changes in acoustic wave velocity (up to 450°C) and sample length (up to 700°C). During the second and third cycles, we measured a strong, reversible increase in wave velocity with increasing temperature (by up to 40% at 450°C): opposite to measurements on granite, and which we interpret as due to crack closure during heating. During cycle one, we detect thermal microcracking within the andesite and the basalt with a low initial microcrack population. For these samples, anomalous thermal expansion during heating is linked to the significant thermal microcracking during cooling. In contrast, the initially highly-microcracked basalt underwent little microcracking throughout. We relate the initial microstructure to the occurrence of thermal microcracking, and explore how rock properties may significantly change with temperature.

Key Points:

- One basalt cracked significantly during cooling, following an anomalous thermal expansion, indicative of stress relaxation, when heated
- All samples see an increase in wave velocity with temperature during repeated heating, attributed to microcrack closure during heating
- Our data literature study suggest low-porosity volcanic rocks with high *P*-wave velocities are most susceptible to thermal microcracking

Supporting Information:

Supporting Information may be found in the online version of this article.

Correspondence to:

L. Griffiths,
luke.griffiths@ngi.no

Citation:

Griffiths, L., Heap, M. J., Lengliné, O., Baud, P., Schmittbuhl, J., & Gilg, H. A. (2024). Thermal stressing of volcanic rock: Microcracking and crack closure monitored through acoustic emission, ultrasonic velocity, and thermal expansion. *Journal of Geophysical Research: Solid Earth*, *129*, e2023JB027766. https://doi.org/10.1029/2023JB027766

Received 30 AUG 2023
Accepted 15 FEB 2024

Author Contributions:

Conceptualization: L. Griffiths, O. Lengliné, P. Baud, J. Schmittbuhl
Data curation: L. Griffiths
Formal analysis: L. Griffiths, H. A. Gilg
Funding acquisition: P. Baud, J. Schmittbuhl
Investigation: L. Griffiths
Methodology: L. Griffiths, O. Lengliné
Project administration: M. J. Heap, P. Baud
Resources: M. J. Heap, P. Baud
Software: L. Griffiths
Supervision: M. J. Heap, P. Baud, J. Schmittbuhl
Visualization: L. Griffiths

1. Introduction

Thermal microcracking influences the physical, mechanical, and transport properties of rock (e.g., C. David et al., 1999; Griffiths et al., 2017; Homand-Etienne & Houpert, 1989; Meredith et al., 2012), and therefore may influence geomechanical behavior and fluid flow within thermally active zones of the subsurface. These zones include geo-engineering sites such as underground disposal facilities for nuclear waste (Faletti & Ethridge, 1988; Hodgkinson et al., 1983) and geothermal reservoirs (Grant, 2013; Huenges et al., 2013; Kolditz et al., 2013; Tomac & Sauter, 2018), as well as natural sites such as volcanoes and fault zones.

Laboratory studies have established the occurrence of microcracking in volcanic rock due to thermal stressing and its significant consequences on rock properties, such as elastic wave velocity and permeability. For example,

Writing – original draft: L. Griffiths
Writing – review & editing: L. Griffiths, M. J. Heap, O. Lengliné, P. Baud, J. Schmittbuhl, H. A. Gilg

Bauer and Handin (1983) measured the thermal expansion coefficient (TEC) of three rocks (Mt. Hood andesite, Cuerbio basalt, and Charcoal granodiorite) during heating to 800°C at a rate of 5°C/min, under confining pressures of 5, 50, and 100 MPa. They found that the thermal expansion of the bulk rock sample was greater than the sum of the individual contributions of each mineral phase, which they attributed to the opening of thermal microcracks during heating. Jones et al. (1997) measured an increase in the permeability of Seljadur basalt (Iceland) following heating to temperatures between 400 and 700°C and cooling (permeability increased by around a factor of nine when heated to 700°C), coinciding with a decrease in the *P*-wave (v_P) and *S*-wave (v_S) velocities. Jones et al. (1997) attributed these results to an increase in microcrack density. Vinciguerra et al. (2005) measured a decrease in v_P of Seljadur basalt by more than 40% following heating to 900°C and cooling, explained by the formation of thermal microcracks. Again, for Seljadur basalt, Nara et al. (2011) measured a permeability increase by almost three orders of magnitude and a decrease in *P*-wave velocity from 5.65 to 4.33 km/s when heated to and cooled from 800°C, owing to thermal microcracking.

However, laboratory studies have also shown that thermal stressing of volcanic rock does not always result in thermal microcracking and therefore has a variable effect on rock properties. For example, Vinciguerra et al. (2005) measured no significant change in the v_P of a basalt from Mt. Etna (Italy) from an initial value of around 3.2 km/s following heating to 900°C and cooling. M. J. Heap et al. (2009) also found no change in the elastic moduli of the same basalt when heated to 900°C and cooled. Vinciguerra et al. (2005) suggested that the high pre-existing crack density within the basalt explained the lack of further thermal microcracking during their experiments. Eggertsson et al. (2020) found that the porosity and permeability of felsite from Krafla volcano (Iceland) was unaffected by thermal stressing when subjected to 15 heating and cooling cycles to a maximum temperature of 450°C. However, these same authors found that the permeability of basalt from Krafla increased by up to an order of magnitude, explained by the absence of pre-existing microcracks compared to the felsite (Eggertsson et al., 2020). Mordensky et al. (2019) found that the porosity and permeability of altered andesites from Mt. Ruapehu (New Zealand) both increased when exposed to high temperature, interpreted as a result of mineralogical changes and thermal microcracking. Weaver et al. (2020) showed that the tensile and compressive strength of hyaloclastite from Iceland increased, and the permeability decreased, following exposure to 600°C. These authors interpreted these changes as a result of the dehydration of the abundant phyllosilicates found within the matrix of the hyaloclastite, rather than due to thermal microcracking. Following exposure to high-temperature, no significant changes were detected either in the physical and mechanical properties of: andesites from Volcán de Colima, Mexico (M. J. Heap et al., 2014; M. J. Heap, Coats, et al., 2018); the strength of dacites from Mt. St. Helens, USA (Kendrick et al., 2013) and Mt. Unzen volcano, Japan (Coats et al., 2018); or the strength of basalt from Pacaya volcano, Guatemala (Schaefer et al., 2015). Considering the above-mentioned studies, the influence of temperature on thermal microcracking and therefore rock properties appears to vary between different volcanic rocks, likely depending strongly on the initial rock microstructure, and the temperature at which measurements are made.

Beyond measurements of physical properties made before and following thermal stressing, acoustic emission (AE; laboratory-scale microseismicity; Lockner, 1993) monitoring is a well-established tool for detecting and characterizing microcracking within rock as it occurs (Abbott et al., 2006; Aker et al., 2014; Baud et al., 2004; Fortin et al., 2006; Glover et al., 1995; Griffiths et al., 2019). Jones et al. (1997) monitored for AE during the heating of Seljadur basalt (Iceland) to 800°C, observing a constant AE rate throughout, which they attributed to thermal microcracking. Vinciguerra et al. (2005) reported AE monitoring data during the heating of Etna basalt (EB) to 600°C and Seljadur basalt to 900°C, in which they observed a continuous increase in the number of AE during heating of the Seljadur basalt, which was highly thermally microcracked upon cooling, and bursts of AE for the EB, which underwent little microcracking. However, until recently, AE monitoring of volcanic rock has been performed during heating, and not during cooling. M. J. Heap et al. (2014) heated and cooled five andesites from Volcán de Colima (Mexico) to a maximum temperature of 450°C whilst monitoring AE. These authors found that AE during cooling, interpreted as thermal cooling microcracks, can be as significant as during heating. Building on this earlier study, Browning et al. (2016) heated and cooled two volcanic rocks (a basalt and a dacite) to a maximum temperature of 1,100°C whilst monitoring AE. These authors detected significantly more AE during cooling, interpreted as due to microcracking. M. Heap, Kushnir, et al. (2018) monitored AE during the heating and cooling of tuff from Mt. Epomeo (Ischia Island, Italy) up to a maximum temperature of 700°C. M. Heap, Kushnir, et al. (2018) detected more AE hits during heating than cooling, likely related to devolatilization reactions. Daoud et al. (2020) heated Slaufrudalar granophyre (Iceland), an andesite from Santorini (Greece), and

the aforementioned Seljadur basalt to temperatures up to 900°C. Thermal stressing of the Slaufrudalar granophyre was characterized by significant AE during heating (interpreted as thermal microcracking) and for the andesite and the microcrystalline basalt, the authors detected few AE during heating, but a significant number of AE during cooling. Daoud et al. (2020) hypothesized that the observed AE during the cooling of the andesite and basalt was the result of thermal cooling microcracks.

However, to monitor microstructural changes, AE monitoring alone is not sufficient. Griffiths et al. (2018) combined AE monitoring and velocity measurements to monitor microcracking during heating and cooling of Westerly granite (USA) samples. They suggested that many AEs recorded during cooling were not associated with the formation of microcracks. Instead, cooling was associated with a repeatable increase in v_P (Griffiths et al., 2018). Furthermore, microstructural changes that do not involve crack extension, including any reversible opening and closing of microcracks, may not be observed through AE monitoring. Due to these factors, and the variability in observations of thermal microcracking in volcanic rocks, an approach combining both velocity and AE monitoring is required to determine the influence of temperature on the microstructure of volcanic rocks.

Here, we selected three volcanic rocks, each with different initial microstructures. We selected a low-porosity, porphyritic basalt from Mt. Etna with 4% porosity (standard deviation of 0.5% across three samples); aphanitic basalt from Rubble Creek in Garibaldi Provincial Park, British Columbia, Canada, with 1% porosity (standard deviation of 0.06% across six samples); and a porphyritic andesite found within the La Lumbre debris-flow track at Volcán de Colima with 23% porosity (standard deviation of 1.1% across eight samples). These materials were selected to provide a variety of porosities and initial microstructures. We heated dry samples of each rock to 450°C, over three heating and cooling cycles under low uniaxial stress, whilst monitoring AE activity and measuring changes in v_P. To help interpret these data, three other samples, prepared from the same sample blocks, were heated to 700°C and cooled over three cycles whilst measuring their elongation.

2. Materials

From blocks of EB, Rubble Creek basalt (RCB) and La Lumbre andesite, three cylindrical samples of each rock (nine total) were cored for the three different heating and cooling experiments (a different sample for each experiment): one for *P*-wave velocity measurement; one for AE monitoring; and one for the TEC measurement. For the wave velocity and AE tests, samples were 40 mm in length and 20 mm in diameter. For the TEC measurements, samples were 10 mm in diameter and 20 mm in length. Samples were dried within a vacuum oven at 40°C for at least 24 hr prior to testing.

Over the past decade, several studies have focused on low-porosity basalt from Mt. Etna: M. J. Heap et al. (2009), Stanchits et al. (2006), Vinciguerra et al. (2005), and Zhu et al. (2016). Mt. Etna is a large and persistently active basaltic stratovolcano at the margin separating the African and Eurasian plates (Bonaccorso et al., 2004). Backscattered Scanning Electron Microscopy (SEM) micrographs of the basalt collected from Mt. Etna and used in this study are shown in Figures 1a and 1b. The basalt has a porphyritic texture consisting of a completely crystallized groundmass hosting pores and phenocrysts. Microcracks, which may be several mm in length, traverse the groundmass (Figure 1a) and phenocrysts (Figure 1b). The connected porosity of the basalt was measured to be around 4% on average (measured by helium pycnometry), and the pores (typically less than 100 microns in diameter) are spread heterogeneously, collected in pockets (Figure 1b). These pockets form the volume between microlites (microscopic crystals) where the groundmass is absent: a diktytaxitic texture (see for example Kushnir et al. (2016)). As a result, the pores are lath-shaped (Figure 1b). The size of the phenocrysts varies from a hundred microns to several millimeters. To further characterize our materials, we measured their thermal diffusivity and thermal conductivity at room temperature with a Hot Disk TPS 500 Thermal Constants Analyzer that utilizes the transient plane source method (see M. J. Heap et al., 2020 for more details). The thermal conductivity and thermal diffusivity of EB was measured to be 1.35 W/m/K and 0.65 mm^2/s, respectively.

An SEM micrograph of a basalt from Rubble Creek is shown in Figure 1c. This basalt has a lower porosity of 1.06% and has an aphanitic texture consisting of a largely crystallized groundmass (similar to the well-studied Seljadur basalt). Rare small crystals (50–200 μm in length) can be found within the microcrystalline groundmass. Few pores are visible. From a qualitative assessment from a series of SEM images similar to those Figure 1, microcracks are thinner and the microcrack density is significantly lower than for the EB (Figure 1c). The thermal conductivity and thermal diffusivity of RCB was measured to be 1.47 W/m/K and 0.74 mm^2/s, respectively.

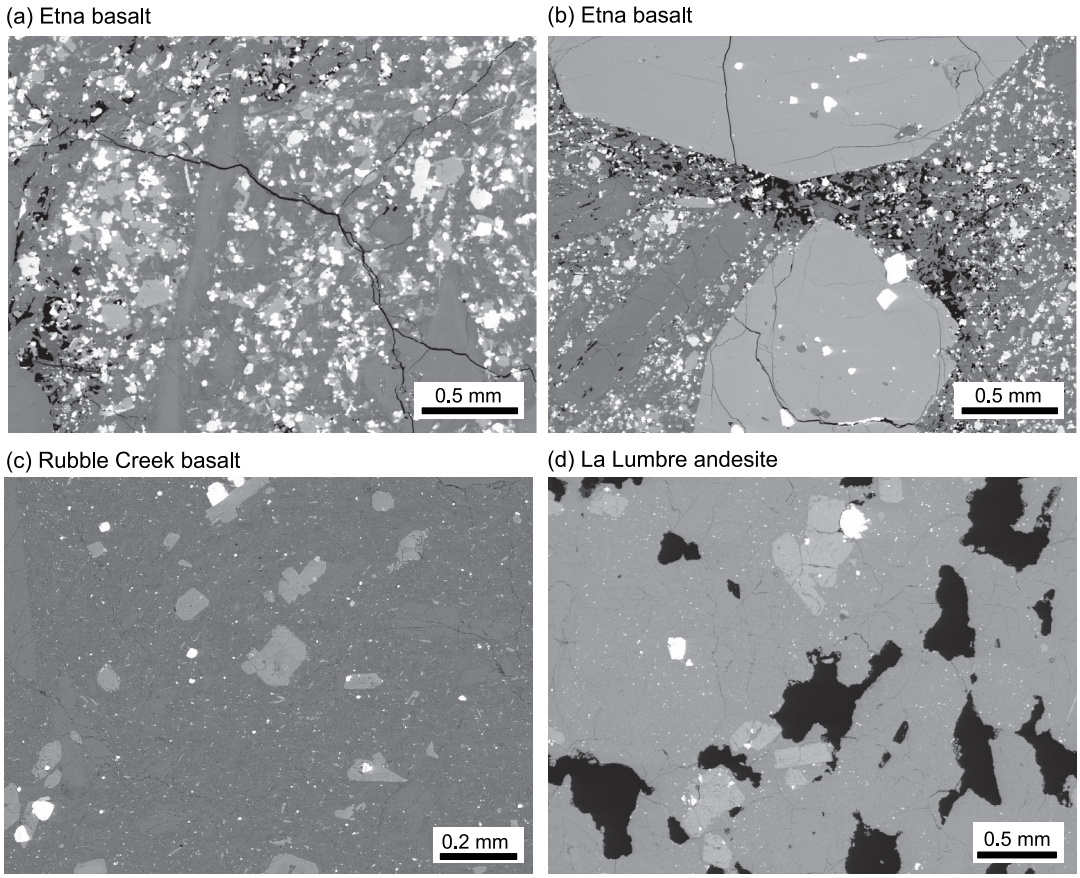

Figure 1. Microstructure of the three volcanic rocks. Backscattered scanning electron microscope micrographs of: (a) the basalt from Mt. Etna containing a microcrack of several millimeters in length and (b) pores collected in pockets; (c) the Rubble Creek basalt; and (d) the La Lumbre andesite from Volcán de Colima (see Farquharson et al. (2017)). Gray—groundmass; Black—void space (pores and microcracks).

An SEM micrograph of the andesite from the Volcán de Colima, an andesitic stratovolcano located within the Trans-Mexican Volcanic Belt (Varley et al., 2019), is shown in Figure 1d (Farquharson et al., 2017). The andesite is a porphyritic, containing phenocrysts within a partially crystallized groundmass (Figure 1d; Farquharson et al., 2017). The andesite has the highest porosity of the three rocks, at around 23%. The andesite contains a glassy groundmass with an abundance of microlites, unlike the basalts which are much more crystallized. The pores within the andesite are irregularly shaped and can be as large as one millimeter across. The groundmass and phenocrysts contain abundant thin microcracks (Figure 1d). The thermal conductivity and thermal diffusivity of the porous andesite from Volcán de Colima was measured to be 0.81 W/m/K and 0.58 mm^2/s, respectively.

Table 1 shows the mineralogical composition of the EB, La Lumbre andesite, and RCB, as determined using X-ray powder diffraction and a Rietveld approach (Doebelin & Kleeberg, 2015). The glass content is determined as the sum of X-ray amorphous phases using ZnO (20 wt.%) as an internal standard. All samples contain a significant and similar amount of plagioclase (44–49 wt.%). The La Lumbre andesite and RCB are glass-rich, 42 and 33 wt.%, respectively. The EB contains no glass but has a larger proportion of crystalline phases including clinopyroxene (25.1 wt.%), olivine (9.9 wt.%), and sanidine (9.3 wt.%). While the feldspathoids cannot coexist with quartz within volcanic rock, the identification of nepheline, leucite and quartz within the EB suggests that the quartz is a secondary mineral or xenocryst.

3. Methods

The experimental setup (Figure 2; Griffiths et al. (2018)) for passive and active acoustic monitoring at high temperature holds a rock sample between two vertical steel pistons within a LoadTrac II servo-controlled uniaxial

Table 1
Mineralogical Composition in wt.% of the Etna Basalt, La Lumbre Andesite, and Rubble Creek Basalt as Determined Using X-Ray Powder Diffraction

Mineral	Etna basalt	La Lumbre andesite	Rubble Creek basalt
Plagioclase (~An50)	44.2	49.3	49.2
Sanidine (Na67)	9.3		
Nepheline	2.7		
Leucite	2.4		
Clinopyroxene	25.1	2.7	1.9
Orthopyroxene			6.4
Olivine	9.9		
Magnetite	4.7	1.5	1.2
F-Apatite	1.0		0.2
Hornblende		2.0	
Chlorite-Smectite		1.0	
Ankerite/Dolomite		0.3	
Tridymite (low)			7.5
Quartz	0.6	0.8	0.7
Amorphous (glass)	0	42.4	32.9
Total	99.7	100.0	100.0

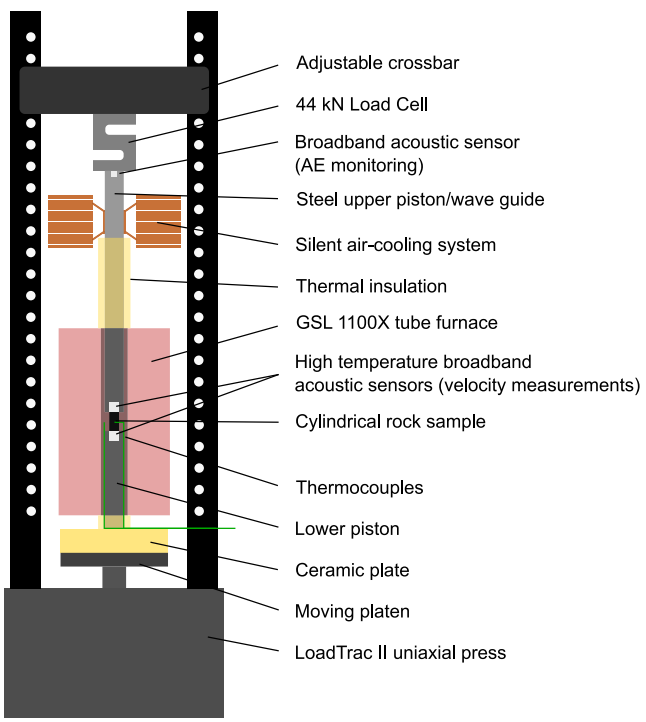

Figure 2. A schematic of the experimental equipment for acoustic emission monitoring and velocity measurements, which combines a LoadTrac II uniaxial press with a GSL 1100X tube furnace. A single acoustic sensor, housed within the top of the upper piston is used for AE monitoring. A pair of high-temperature sensors, embedded within the top and bottom pistons and in direct contact with the sample, are used for *P*-wave travel time measurements (modified from Griffiths et al. (2018)).

press. The sample is contained within a GSL-1100X tube furnace (MTI Corporation). The furnace has an 80 mm height constant temperature zone, thus covering the entire sample length. Temperature was measured using a thermocouple held at 1 cm from the sample surface at its mid-height. All reported temperatures were measured using this thermocouple. An AE transducer is embedded within the upper piston and is kept cool, along with the load cell, using an air-cooling system attached around the top of the upper piston.

3.1. Heating and Cooling Rates

Dry samples were heated to 450°C and cooled at a rate of 1°C/min, with a 2-hr dwell time at the peak temperature. Throughout the heating and cooling, a uniaxial stress of 0.3 MPa was maintained on the sample. The heating rate, selected to limit thermal gradients within the sample, is lower or in line with those used in previous experimental studies of thermal microcracking in rock (e.g., Browning et al., 2016; H. F. Wang et al., 1989; X.-Q. Wang et al., 2013). To determine the thermal gradient within the samples, we can use the analytical expressions for the temperature change over time within an infinite cylinder following a change in temperature at its surface (Cengel & Ghajar, 2010). Figure 3 shows the temperature change against distance from the cylinder axis after a sudden 1°C increase in surface temperature. The temperature change throughout the sample is given at 30, 60, 90, 120, and 180 s following the temperature increase, assuming the thermal properties of the RCB. We see that, following an increase in temperature of 1°C, the temperature at the center of the sample has increased by almost 0.9°C after 60 s and that thermal equilibrium is achieved after 180 s. These results confirm that heating and cooling rates of 1°C/min are sufficiently low to consider the samples at thermal equilibrium during the experiments presented in this study.

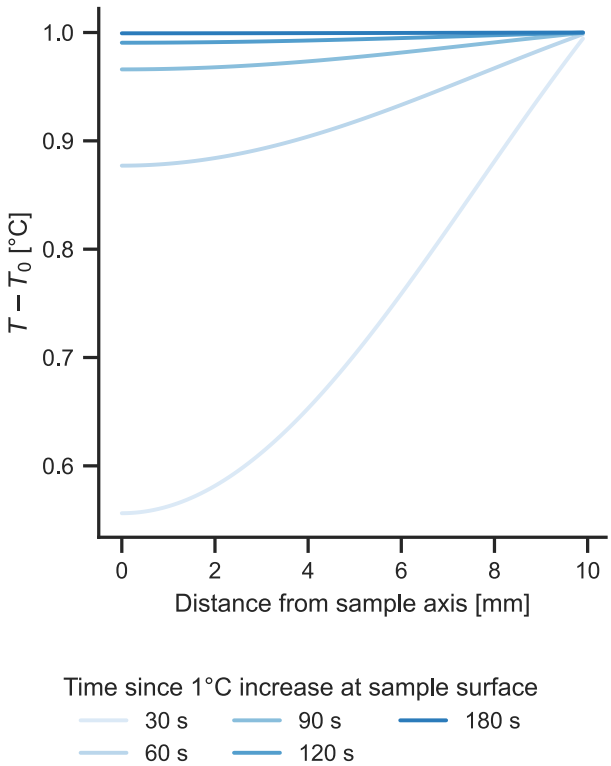

Figure 3. Evolution of the temperature profile within an infinite cylinder of thermal diffusivity 0.74 mm^2/s (that of the Rubble Creek basalt) subject to an increase in surface temperature of 1°C. T is the temperature within the sample and T_0 is the initial sample temperature.

As further confirmation of this analysis, we may use the method described in X.-Q. Wang et al. (2013) to determine the time constant, t, needed for the thermal equilibration. This constant is given by $t = r^2/d$, where d is the thermal diffusivity and r is the sample radius. For the samples used in this study (i.e. $r = 1 \times 10^{-2}$ m), the thermal time constant is 153, 135, and 172 s considering the thermal diffusivities of the EB, RCB, and La Lumbre andesite, respectively. For the TEC measurements performed on smaller samples (described below), the time constants are 38, 34, and 43 s for the respective materials. These calculations are conservative due to the assumption that all heat diffuses radially; in practice heat flows through the faces of the cylindrical sample, leading to quicker thermal equilibration. Thus, our imposed heating/cooling rates are close to the rates needed for thermal equilibration of the sample.

3.2. Active and Passive Acoustic Monitoring

P-wave velocities were measured during heating and cooling using two high-temperature acoustic sensors housed within each piston and in direct contact with the opposing faces of the samples (Figure 2). The high-temperature sensors were the 9,215 sensors from Physical Acoustics, with a resonant frequency of 100 kHz (52 dB) and operating frequency in the range of 80–560 kHz. Coupling with the sample was ensured, and kept constant by, a servo-controlled axial stress of about 0.3 MPa. A signal generator was connected to the upper transducer and programmed to emit a 200 kHz sinusoidal pulse once every 50 ms. A National Instruments BNC 2110 acquisition card was used to record the amplified (with a +40 dB preamplifier 2 kHz high pass filter) voltage at the receiver transducer. The recorded voltage waveforms had a duration of 2 ms (including a 0.05 ms pre-trigger recording time) and sampling frequency of 2 MHz. To increase the signal-to-noise ratio waveforms were stacked 50 times, with a waiting time of 10 s between stacks. Acquisition was performed continuously during the three heating and cooling cycles.

Figure 4 shows the acquired waveform amplitudes with time alongside the furnace temperature. Aside from the first heating of the RCB, where the travel time is near unchanged, the overall trend is one of decreasing wave travel time with increasing temperature (shifting of wave amplitudes to the left at higher temperatures). The waveform amplitudes and arrival times show little variation once the furnace temperature reaches the target temperature, implying that the sample quickly reaches thermal equilibrium when heated and cooled at 1°C/min.

P-wave arrival times were determined from the time shift of the *P*-wave first arrivals. Using only the first 30 μs of the recorded waveforms, cross-correlation functions were calculated between waveforms pairs (without interpolation). Next, the cross-correlation functions for each pair were interpolated using piecewise quadratic interpolation around their maximum, and the final time shift was taken to be the maximum of the newly interpolated function. *P*-wave velocities were calculated from the cumulative shift in *P*-wave travel time, the initial *P*-wave travel time (corrected for the travel time within the sensor housing) and the initial sample lengths measured prior to the experiments. Considering the sampling frequency of 2 MHz, sample length of 40 mm, and 0.01 mm precision of the calipers to measure the sample length, the precision in velocity measurement is ±125 m/s for samples with a velocity of 4,500 and ±40 m/s for velocities of 1,750 m/s.

For the AE monitoring experiments, samples were heated to and cooled from 450°C at a rate of 1°C/min, with a 2-hr dwell time at the maximum temperature. A broadband AE sensor was housed facing toward the sample within the center of the upper piston (to best capture the AE energy). The piston, which forms a continuous waveguide and thus limits the attenuation at surface interfaces, was used to apply a servo-controlled axial stress of about 0.3 MPa. A servo-controlled load ensures that the stress on the sample does not change during heating and cooling as the sample and pistons expand and contract, respectively. A micro80 miniature AE sensor (200–900 kHz bandwidth and a 325 kHz resonant frequency) from Physical Acoustics was used in conjunction with a 1283 USB AE Node (a single-channel AE digital signal processor with a built-in 26 dB preamplifier and low- and high-pass

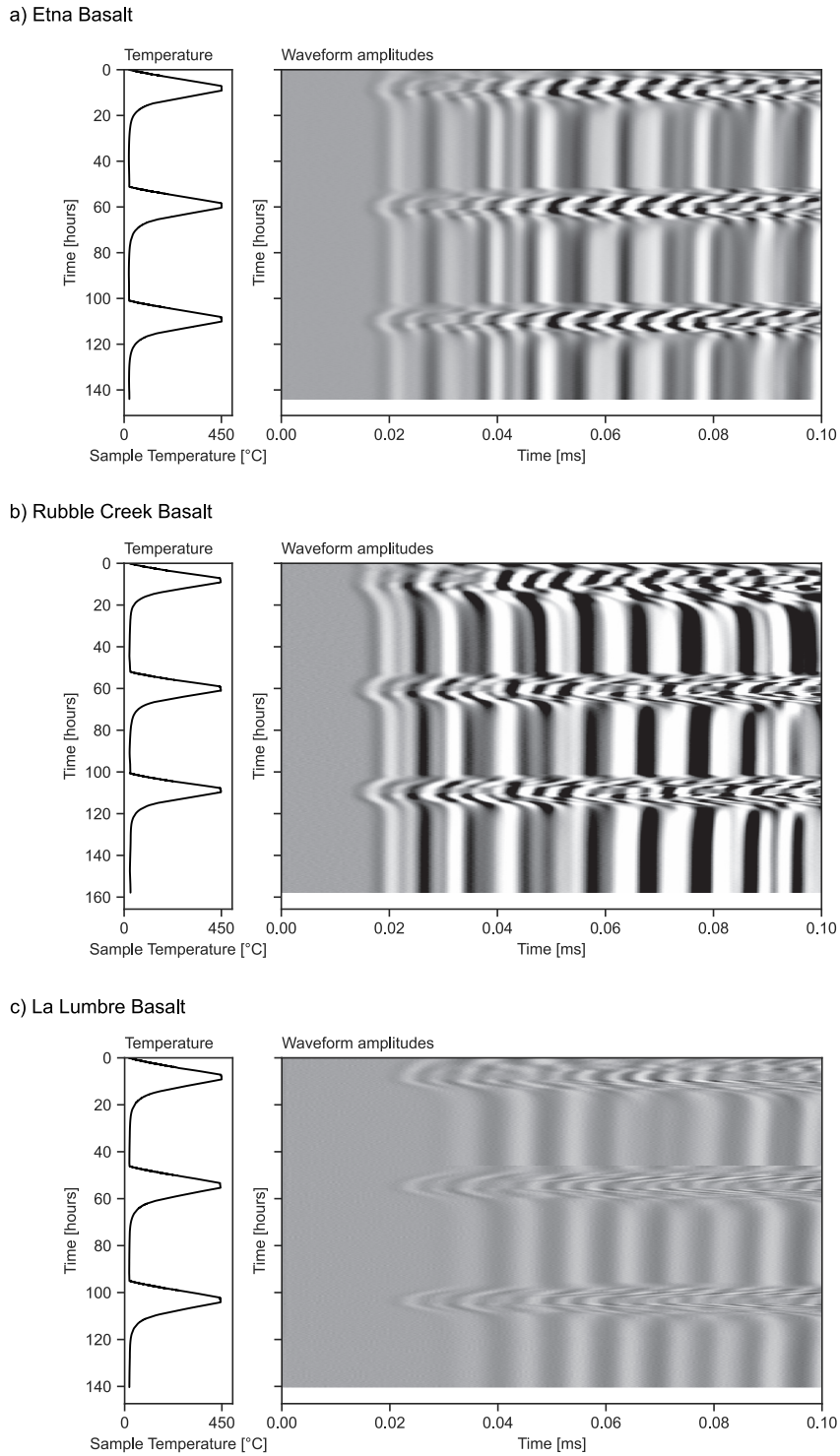

Figure 4. Furnace temperature and waveform amplitudes recorded during the repeated heating and cooling experiments on samples of (a) Etna basalt, (b) Rubble Creek basalt, and (c) La Lumbre andesite.

analog filters 20 kHz and 1 MHz, respectively). An AE "hit" was registered when the pre-amplified voltage across the transducer crossed the 40 dB detection threshold (with respect to a 1 μV reference voltage). The trigger parameters of the 1283 USB AE Node were set to 400 μs for the peak definition time (the maximum time following triggering before which the peak voltage may be determined), 400 μs hit definition time (the maximum

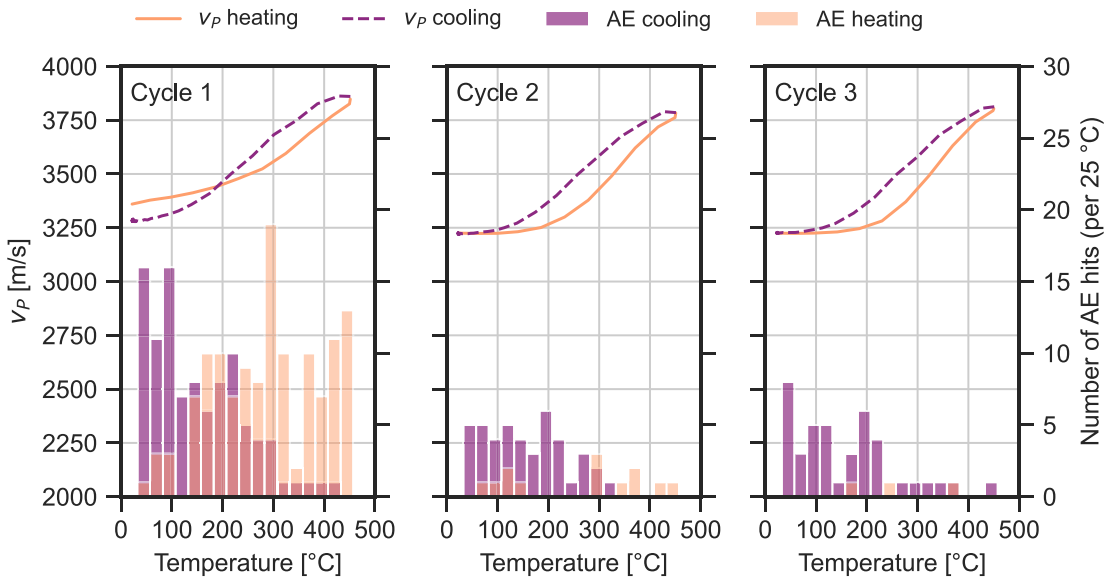

Figure 5. Passive and active acoustic monitoring of Etna basalt during thermal stressing: *P*-wave velocity (v_P) and number of acoustic emissions detected during three cycles of heating and cooling to a peak temperature of 450°C.

time between consecutive threshold crossings, above which they are considered as part of separate hits), and a 1,000 μs hit lockout time (the minimum time between consecutive hits). These parameters were selected to correctly capture the AE produced by a Hsu-Nielson source (pencil lead break) on the surface of the sample when mounted in the uniaxial press. The detection threshold was adjusted to be above the mechanical and electrical noise level of the system. When triggered, the 1283 USB AE Node also recorded the first 7 ms of each AE waveform (7,000 time samples at 1 MHz sampling rate) with a 100 μs pre-trigger. An AE monitoring experiment was performed on a sample of fused quartz to ensure that no significant number of AE were recorded throughout a heating and cooling cycle.

Although it is technically feasible to combine active and passive acoustic measurements within a single experiment, the chosen methodology involves conducting separate experiments to ensure low and consistent AE detection thresholds. This approach leverages the high sensitivity of the broadband AE sensor, which is superior to the high temperature sensors used for active monitoring, and a cooling system to ensure a stable response. Finally, it prevents the data loss associated with interference between active and passive measurements.

3.3. Thermal Expansion Coefficient Measurement

Measurements of the sample elongation (linear thermal expansion) with temperature were performed by ELEMCA, France, using a TMA 402 F1 Hyperion Thermomechanical Analyzer. The analyzer is a vertical dilatometer which measures sample elongation (linear thermal expansion) with temperature, providing the TEC as a function of temperature. The resolution of the elongation measurement is 0.01 μm and the precision is verified to be ±0.02 μm during calibration. Measurements were performed in a helium atmosphere. Samples were first left to stabilize at room temperature for 15 min, then heated to 700°C at a rate of 5°C/min. Samples stabilized at 700°C for 5 min, then were cooled at 5°C/min, before a final stabilization period of 15 min at room temperature °C. This procedure was repeated three times for each sample.

4. Results

4.1. Active and Passive Ultrasonic Monitoring During Three Heating/Cooling Cycles

Figures 5–7 show the *P*-wave velocity measurements and AE rate (per 25°C) during three heating and cooling cycles to a maximum temperature of 450°C for samples of each rock. While velocities were calculated using a constant sample length as measured prior to each cycle, we consider the influence of sample elongation on the

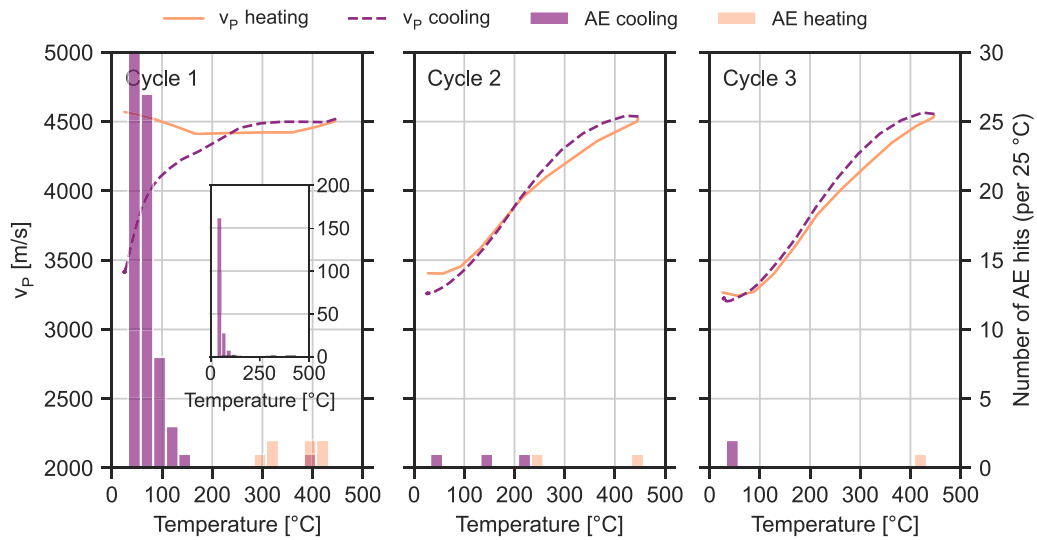

Figure 6. Passive and active acoustic monitoring of Rubble Creek basalt during thermal stressing: *P*-wave velocity (v_P) and number of acoustic emissions (AE) detected (per 25°C) during three cycles of heating and cooling to a peak temperature of 450°C. The AE scale is cut for cycle 1, and the peak AE rate is shown in the inset graph.

velocity to be negligible, as the measured thermal expansion of the samples was low compared to the relative change in travel time (<0.3% for Rubble Creek and Etna basalts, and <0.6% for the andesite at 450°C; Figure 9).

For the EB, during the first heating phase v_P increased from 3,360 m/s at room temperature to 3,860 m/s at 450°C (~15% increase; Figure 5). The temperature for the onset of AE during heating is around 120°C, above which about 8 AE hits were detected per 25°C. During cooling v_P decreased from 3,860 m/s at 450°C to 3,290 m/s at room temperature, resulting in a permanent decrease in v_P of 70 m/s (~2% of the initial velocity). In total, 130 AE hits were detected during heating and 100 AE hits were detected during cooling. For cycles 2 and 3, no permanent change in velocity was observed and fewer AE were detected than for the first cycle: 13 during heating and 43 during cooling for cycle 2; and 3 during heating and 41 during cooling for cycle 3. During cycles 2 and 3, the *P*-

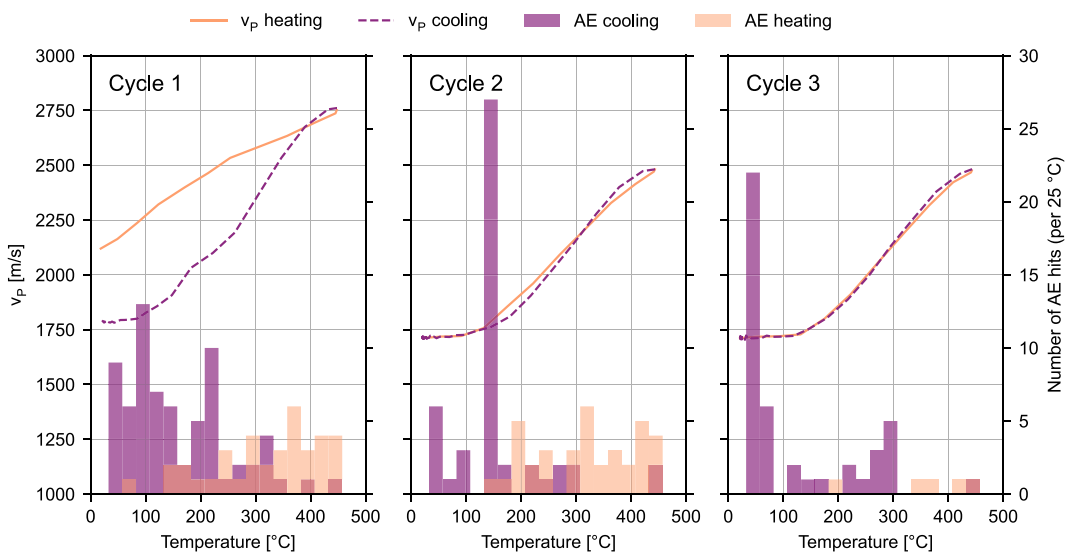

Figure 7. Passive and active acoustic monitoring of La Lumbre andesite during thermal stressing: *P*-wave velocity (v_P) and number of acoustic emissions (AE) detected (per 25°C) during three cycles of heating and cooling to a peak temperature of 450°C.

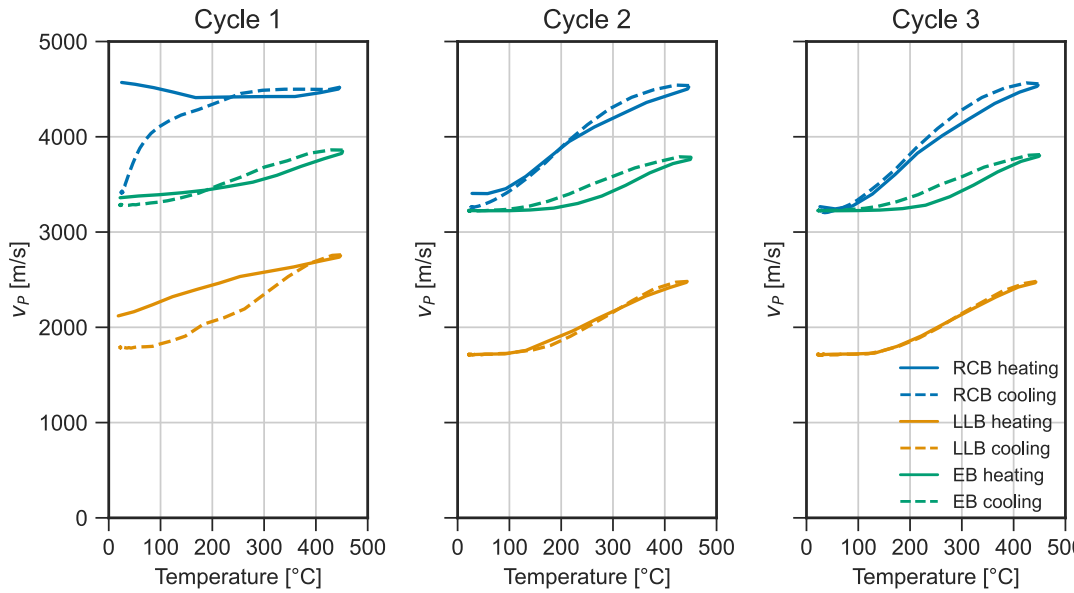

Figure 8. Evolution of *P*-wave velocity (v_P) of the Rubble Creek basalt, La Lumbre andesite, and Etna basalt with temperature during three heating and cooling cycles to a peak temperature of 450°C.

wave velocity of EB increases significantly as a function of increasing temperature, from ~3,260 m/s at room temperature to ~3,800 m/s at a temperature of 450°C (~15% increase; Figure 5). However, during the repeat cycles, no permanent changes in v_P were observed.

As the RCB was heated for the first time, 7 AE hits were detected during heating (from about 300°C, and v_P decreased from 4,570 m/s at room temperature to 4,410 m/s at 170°C, Figure 6). However, during heating between 170 and 360°C, v_P of the RCB was near-constant, reaching 4,520 m/s at 450°C. During cooling, v_P remained near constant until around 250°C, at which point v_P started to decrease. From 120°C to room temperature there was a strong decrease in v_P to 3,420 m/s (a 25% decrease from the initial value), accompanied by a high AE rate, with 202 hits in total detected during cooling (Figure 6). Very few AE hits were detected during the second and third cycles: 5 during cycle 2, and 3 during cycle 3. The net decrease in velocity was only 136 m/s during cycle 2, and 35 m/s during cycle 3. Cycles 2 and 3 show large differences in v_P as a function of increasing temperature, and a similar evolution of velocity during both cycles. In cycle 3, for example, v_P was 3,225 m/s at room temperature and 3,795 m/s at a temperature of 450°C (~38% increase; Figure 6). The permanent decreases to v_P were small following cycles 2 and 3.

For the La Lumbre andesite during the first cycle, v_P increased with increasing temperature, from 2,120 to 2,760 m/s at 450°C (Figure 7). During cooling v_P decreased to 1,790 m/s, significantly lower than the initial velocity. 37 AE hits were detected during heating of cycle 1, with the onset of AE during heating occurring at around 120°C, and above which about eight hits were detected per 25°C. 70 AE hits were detected during cooling, in particular between 250°C and room temperature. Between cycles 1 and 2 there is a slight decrease in velocity of about 50 m/s which occurred during the period of a few hours between the two cycles. During cycles 2 and 3, v_P increased reversibly to 2,480 m/s at 450°C, and fewer AE hits were detected than during the first cycle (37 during heating of cycle 2 and 48 during cooling, and five during heating of cycle 3 and 44 during cooling). As for the EB and RCB, cycles 2 and 3 show that, even in the absence of significant microcracking, v_P is temperature dependent: v_P increases from 1,715 m/s at room temperature to 2,480 m/s at a temperature of 450°C (~43% increase; Figure 7).

Figure 8 shows the evolution of v_P for all samples as a function of temperature during cycles 1 to 3. The La Lumbre andesite has the lowest initial velocity, and the RCB has the highest initial velocity. During cycle 1 all rocks see a hysteretic evolution of velocity with temperature, resulting in a permanent decrease in velocity following heating and cooling, and most significant for RCB and La Lumbre andesite. The velocities of the EB and La Lumbre andesite both increased during heating and decreased during cooling, and the velocity of the RCB decreased during both heating and cooling. For each sample, the velocity changes with temperature during cycles

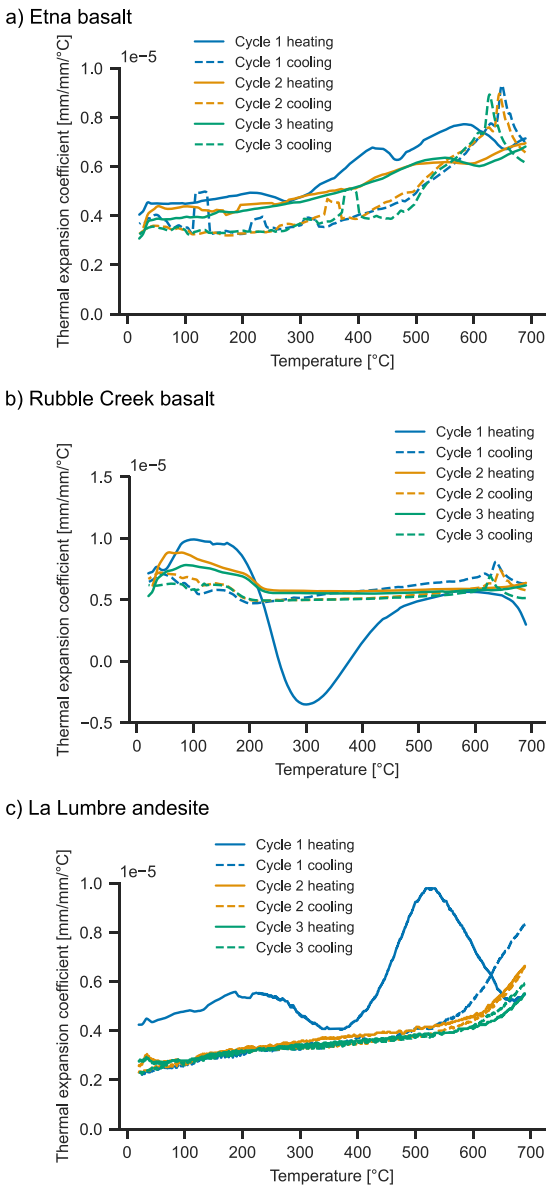

Figure 9. Thermal expansion coefficient against temperature for (a) Etna basalt, (b) Rubble Creek basalt, and (c) La Lumbre andesite. Measurements were made over three heating (solid lines) and cooling (dashed lines) cycles up to a peak temperature of 700°C.

2 and 3 are near identical: the velocity increase during heating was almost entirely reversed during cooling (Figure 8).

4.2. Thermal Expansion During Three Heating/Cooling Cycles

The TEC during heating and cooling are provided for each sample in Figures 9–11. The values of relative length change with temperature are provided in Figure S1.

Figure 9a shows for EB the (TEC) during heating and cooling over three cycles to a maximum temperature of 700°C. Throughout the heating and cooling cycles, the TEC is positive. The TEC ranges from about 0.4×10^{-5} mm/mm/°C close to room temperature, to about 0.7×10^{-5} mm/mm/°C close to 700°C. The TEC values during all cooling cycles, and heating cycles 2 and 3, are very similar. The TEC during heating of cycle 1 is consistently greater than the values measured during heating cycles 2 and 3. The inflexion observed during cooling at around 700°C is an artifact due to a loss of heating control. During cooling, a transition is visible between temperatures of about 600 and 500°C leading to a lower TEC.

For the RCB (Figure 9b), we observe a strong decrease in TEC during the first cycle, where it becomes negative between about 250 and 350°C. Such behavior is generally interpreted as stress relaxation, whereby, at sufficiently high temperatures, internal stresses are relieved through plastic deformation of the material. During cooling the TEC is hysteretic and does not follow the inflexion observed during heating, remaining at around 0.5×10^{-5} mm/mm/°C throughout. As for the EB, TEC values during all cooling cycles, and heating cycles 2 and 3, are very similar. Again, as for the EB, the inflexion observed during cooling at around 700°C is an artifact due to a loss of heating control.

For the La Lumbre andesite (Figure 9c) the TEC is about 0.4×10^{-5} mm/mm/°C around room temperature during the first heating cycle. This is followed by a decrease in TEC (from around 250–450°C), and an increase and peak at around 520°C. As for the previous samples, TEC values during all cooling cycles, and heating cycles 2 and 3, are very similar. The values during cooling are lower than those during the heating stage of the first cycle.

5. Discussion

5.1. Observations of Thermal Microcracking

5.1.1. Thermal Microcracking During Cooling

During cycle 1, for the EB (~4% porosity) and La Lumbre andesite (~23%) we observe an increase in v_P during heating (Figures 5 and 7). For the RCB (~1% porosity), v_P is near constant throughout heating (Figure 6). For all samples, there is little AE during heating of the first cycle (Figures 5–7). Due to the limited number of AE and absence of a velocity decrease, we do not expect microcracking to have occurred in the RCB during heating of the first thermal stressing cycle.

For all samples, during cooling on the first cycle, we measured a decrease in v_P, leading to a net decrease over the first cycle (Figures 5–7): large decreases in velocity were observed for the RCB (Figure 6) and La Lumbre andesite (Figure 7), and a small decrease for EB (Figure 5). A permanent decrease in v_P is an expected result of thermal microcracking (e.g., Nara et al., 2011; O'Connell & Budiansky, 1974; Schubnel et al., 2006; Stanchits et al., 2006). For the RCB, the strong increase in the number of AE and a large decrease in v_P toward the end of the cooling (Figure 6) also suggest that significant microcracking occurred as the sample first cooled. A permanent decrease in v_P was observed also for the La Lumbre andesite (Figure 7), indicative of thermal microcracking. For

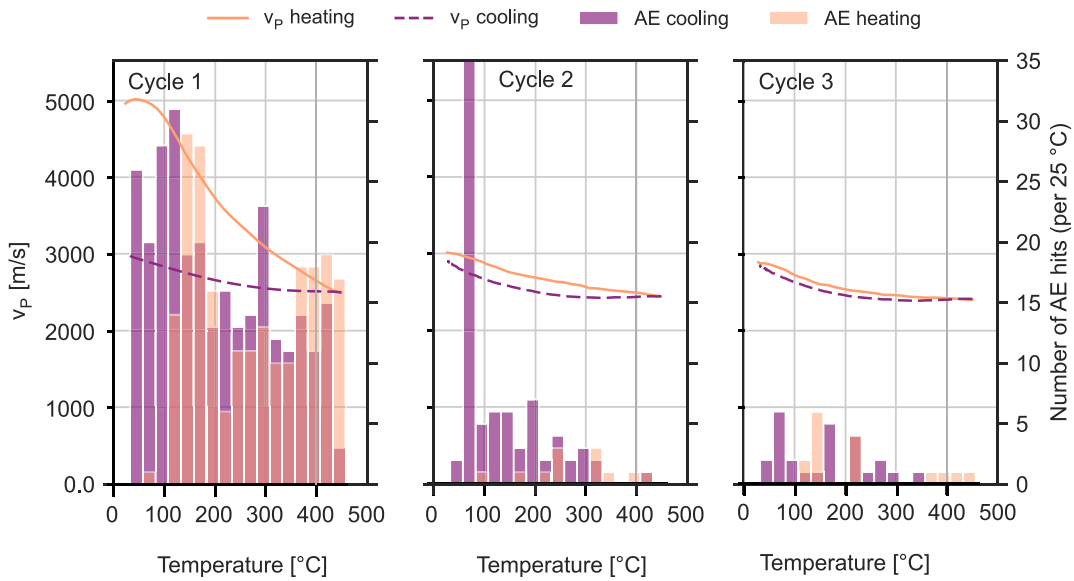

Figure 10. Passive and active acoustic monitoring of Westerly granite during thermal stressing: *P*-wave velocity (v_P) and number of acoustic emissions detected during three cycles of heating and cooling to a peak temperature of 450°C (data from Griffiths et al. (2018)).

the EB (Figure 5), the final v_P is similar to the initial value, and therefore we expect little microcracking occurred during the first cycle. The TEC measurements (Figure 9) also provide an indication of when thermal microcracking occurs. Specifically, for the La Lumbre Andesite throughout cooling, and for the RCB when cooling from 200°C to room temperature, the thermal expansion coefficients are lower compared to the values measured at the same temperatures during heating. This reduction in TEC during cooling is an indication of microcrack opening, analogue to the microcrack opening observed in granite when heated (Cooper & Simmons, 1977).

Contrary to studies of thermal microcracking in granite (Griffiths et al., 2018; H. F. Wang et al., 1989; Yong & Wang, 1980), and in particular for the RCB, here we detect a significantly greater number of AE during cooling than during heating. M. J. Heap et al. (2014), Browning et al. (2016), and Daoud et al. (2020) measured the output of AE during the heating and cooling of volcanic rocks, and also found that AE activity can be significant during cooling. Browning et al. (2016) performed AE monitoring during a single heating and cooling cycle (to a peak temperature of 1,100°C) of a basalt from Seljadur and a dacite from Nea Kameni (Santorini), and Daoud et al. (2020) heated Slaufrudalar granophyre, an andesite from Santorini, and Seljadur basalt to progressively higher temperatures (up to 700°C). These authors found that for all rocks except the granophyre, both the AE rate and the AE energy of hits were greater during cooling than during heating, suggesting that thermal microcracking occurred predominantly during cooling. However, we note that the studies by M. J. Heap et al. (2014), Browning et al. (2016), and Daoud et al. (2020) did not also measure v_P during heating and cooling, and AE data alone should be treated with caution. For example, our data for EB show that AE need not be associated with significant microcracking. Our results highlight the need for simultaneous AE and v_P measurements for understanding the complex behavior of volcanic rocks during heating and cooling cycles.

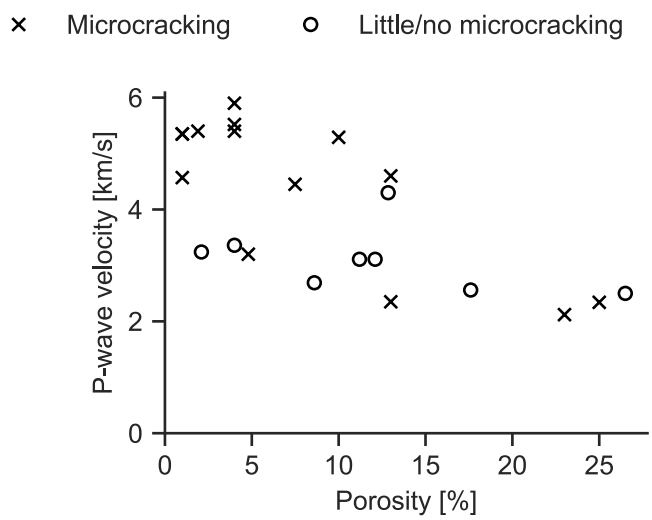

Figure 11. *P*-wave velocity measured prior to heating as a function of porosity for volcanic rocks from the selected studies in Table 2. Crosses are for samples which underwent thermal microcracking when heated and cooled, and circles are for samples which did not undergo microcracking. Where ranges of values are given for a study, the mid-range value is taken.

5.1.2. Absence of Microcracking During Repeated Heating and Cooling

For all samples, during the repeated heating and cooling cycles 2 and 3, we observed a strong and reversible increase in *P*-wave velocity with increasing

temperature (by up 40% at 450°C; Figure 8) and only few AE (Figures 5–7). In the thermal expansion data, we observe for each sample a positive and monotonous TEC with increasing temperature (Figure 9). The reversible change in TEC and velocity, and the absence of significant AE, suggest that little thermal microcracking occurred within the samples during cycles 2 and 3. Exceptions to this general trend would be during the La Lumbre Andesite experiment, where larger numbers of AE were detected at about 150°C during cooling of cycle 2, and near room temperature during cooling of cycle 3 (Figure 7). However, as these hits did not coincide with a change in wave velocity, we do not interpret these AE hits as thermal microcracking. Instead, we attribute them to localized damage observed at the sample ends, where the edges cut through large pores and weaken the rock structure.

For all rocks studied here, the quasi-reversible change in velocity with temperature during cycles 2 and 3 (Figure 8) is evidence that very little thermal microcracking occurred after cycle 1. This behavior is a thermal analog to the Kaiser stress-memory effect (Kaiser, 1953), whereby a material does not undergo further damage when subject to mechanical stresses it has already experienced. This behavior has previously been observed in the laboratory during the repeated thermal stressing of rocks including granite (Atkinson et al., 1984; Griffiths et al., 2018), and manufactured materials such as concrete (M. J. Heap et al., 2013). Recently, Daoud et al. (2020) showed for three volcanic rocks that AE activity during thermal cycling recommences only once the peak temperature reached during a previous cycle has been exceeded—an observation in agreement with the thermal Kaiser stress-memory effect. For the EB, very little thermal microcracking occurred during cycle 1, perhaps due to the extensive pre-existing network of microcracks (Vinciguerra et al., 2005). The thermal Kaiser effect is likely applicable to volcanic rocks more generally, as multiple studies have suggested that an initially high microcrack content may limit thermal stress build-up and further damage within volcanic rock (Coats et al., 2018; M. J. Heap, Coats, et al., 2018; Vinciguerra et al., 2005).

We note that in this study and those mentioned above, the duration and number of cycles are limited, and that thermal stress fatigue may arise over many thermal stress cycles and eventually lead to rock breakdown (Hall & Thorn, 2014). Another potentially influencing factor is the rate of heating and cooling rate. For granite, faster cooling (e.g., through submersion in cool water) may result in increased microcrack damage (Eggertsson et al., 2020; Siratovich et al., 2011; Zhang et al., 2018). When cooled rapidly, the temperature gradients within the rock result in higher thermal stresses and enhanced microcracking, even if the sample has previously been cooled from the same temperature. For volcanic rocks, Eggertsson et al. (2020) quench-cooled samples of basalt from Krafla in water (from 450°C) and measured higher permeability values for these than for samples that were cooled from 450°C in air or at a controlled rate of 5°C/min, suggesting that quench-cooling resulted in the development of more microcracks. Faster cooling may not always be sufficient, however: M. J. Heap, Coats, et al. (2018) heated samples of low-porosity andesite to 700°C and quench-cooled them in water, resulting in no change in the physical properties of the rock.

5.2. Structural Relaxation Leading to Thermal Microcracking During Cooling

Theoretical studies have proposed micromechanical models to explain thermal microcracking in crustal rock (Fredrich & Wong, 1986; Meredith et al., 2001), whereby the mismatched thermal expansion between neighboring grains during heating results in a build-up of mechanical stresses and the propagation of fractures once a certain temperature threshold is reached. Such studies have focused on the formation of microcracks within rocks including granite, diabase, limestone, and quartzite, and their models are applicable to granular materials in which microcracks are shorter than the grain size. In granular geomaterials, thermal microcracks formed during heating first occur along grain boundaries and intragranular microcracks occur at higher temperatures (Fredrich & Wong, 1986; Isaka et al., 2019). These models, which consider stress change as a function of an increase in temperature, are not sufficient to predict the cooling-dominated microcracking observed here (in particular for the RCB; Figure 5).

Daoud et al. (2020) heated samples of Santorini andesite and Seljadur basalt, which have a micro-crystallized groundmass, over multiple heating cycles to peak temperatures of 350, 500, 700, and 900°C. These authors observed AE mostly during cooling (more details in Table 2) once samples had been heated to a temperature exceeding 500°C. During heating, the AE rate and AE energies were lower than during cooling—explained by Daoud et al. (2020) as resulting from small increments in crack extension of crystal boundary cracks (within the microcrystalline groundmass). The high energy AE during cooling is explained by these authors as the growth of

Journal of Geophysical Research: Solid Earth

10.1029/2023JB027766

Table 2
Literature Review of Laboratory Studies of Thermal Microcracking in Volcanic Rock

Rock (reference)	Location	Porosity (%)	*P*-wave velocity (m/s)	Rock groundmass	Phenocrysts	Presence of pores	Initial presence of microcracks	Heating temperature (°C)	Observations	Occurrence of thermal microcracking
Basalt (this study)	Mt. Etna, Italy	~4	3,360	Crystallized groundmass	Yes (up to several mm)	Some pores (<100 mm)	Yes	450°C	AE observed. Near reversible velocity change during heating/cooling	No/very little
Rubble Creek basalt (this study)	Garibaldi Provincial Park, British Columbia, Canada	~1	4,570	Crystallized groundmass	Yes (<0.2 mm)	No pores	Yes	450°C	Significant AE during cooling. Decreased v_P	Yes
La Lumbre andesite (this study)	Volcán de Colima, Mexico	~23	2,120	Glass	Yes (<1 mm)	~0.1–1 mm	Yes	450°C	Significant AE, decreased v_P	Yes
Basalt (Browning et al., 2016)	Seljadur, Iceland	~4	5,520	Tholeitic	mean grain size 80 μm	Small pores <0.2 mm	Yes	900°C	AE (mostly during cooling)	Yes
Dacite (Browning et al., 2016)	Nea Kameni, Santorini	~10	5,290	Crystallized groundmass	Yes (~500 μm)	Large pores (up to around 1 mm)	Yes	900°C	AE (mostly during cooling)	Yes
Andesite (M. Heap, Kushnir, et al., 2018)	Volcán de Colima, Mexico	0.7–0.9	–	Crystallized groundmass	Yes (<1 mm)	Many small pores <10 μm	Yes (100–1,000) μm	400–700°C	No difference in strength, stiffness, permeability following heating	No
Andesite (Li et al., 2019)	Déhaies, Guadeloupe	1.5–2.3	5,400	Crystallized groundmass	Yes (mean 0.1 mm)	Some pores (0.5–10 μm)	Yes (300–500 μm)	500, 800, 930, 1,100°C	>800 C increase in crack density and permeability decrease in v_P	<500 C No, 800–1,100 Yes
Basalt (Vinciguerra et al., 2005)	Seljadur, Iceland	1	5,280–5,420	Tholeitic	Yes	Some pores (<100 μm)	Yes	900°C	Decrease in v_P, increase in permeability	Yes
Basalt (Vinciguerra et al., 2005)	Mt Etna, Sicily, Italy	2.10	3,050–3,430	Crystallized	Yes	Few pores (<50 μm)	Yes	900°C	Negligible change in v_P and permeability	No
Basalt (Jones et al., 1997, same as in Vinciguerra et al., 2005)	Seljadur, Iceland	See Vinciguerra et al. (2005)	See Vinciguerra et al. (2005)	Tholeitic	Yes	0.05–0.25 mm	N/A	800°C	AE, v_P decrease, Permeability increase	Yes
Basalt Nara et al. (2011): not from the same block as Vinciguerra et al., 2005)	Seljadur, Iceland	4	~5,900 km/s at 5 MPa	Glassy matrix, tholeitic	Yes	Yes	No visible microfractures	600, 800	Decrease in v_P, increase in permeability	Yes
Andesite (Siratovich et al., 2014, 2015)	Rotokawa, New Zealand	5.3–20.4	4,100–4,500	Crystallized	Yes	Many small and large pores (up to	Yes	350, 900°C	No hysteresis in thermal expansion	No
Andesite (B5) (M. J. Heap et al., 2014)	Volcán de Colima Mexico	12.10	3,110	Crystallized, containing interstitial glass	Yes (<1.5 mm)	Yes, mean equivalent radius 0.0690 mm	Yes	450°C	Decrease in v_P of 400 m/s, little change in measured crack density	No/little
		8.60	2,690				Yes	450°C		No/little

Journal of Geophysical Research: Solid Earth

10.1029/2023JB027766

Table 2
Continued

Rock (reference)	Location	Porosity (%)	*P*-wave velocity (m/s)	Rock groundmass	Phenocrysts	Presence of pores	Initial presence of microcracks	Heating temperature (°C)	Observations	Occurrence of thermal microcracking
Andesite (B4) (M. J. Heap et al., 2014)	Volcán de Colima Mexico			Crystallized, containing interstitial glass	Yes (<1.5 mm)	Yes, mean equivalent radius 0.0855 mm			Decrease in v_P of 170 m/s, little change in measured crack density	
Andesite (A5) (M. J. Heap et al., 2014)	Volcán de Colima Mexico	11.20	3,110	Crystallized, containing interstitial glass	Yes (<1.5 mm)	Yes (mean equivalent radius 0.1136 mm)	Yes	450°C	Decrease in v_P of 260 m/s, little change in measured crack density, AE during heating and cooling	No/little
Andesite (C8) (M. J. Heap et al., 2014)	Volcán de Colima Mexico	17.60	2,560	Crystallized, containing interstitial glass	Yes (<1.5 mm)	Yes (mean equivalent radius 0.1248 mm)	Yes	450°C	Decrease in v_P of 250 m/s, little change in measured crack density, AE during heating and cooling	No/little
Andesite (LAH4) (M. J. Heap et al., 2014)	Volcán de Colima Mexico	25	2,340	Crystallized, containing interstitial glass	Yes (<1.5 mm)	Yes (mean equivalent radius 0.1028 mm)	Yes	450°C	Decrease in v_P of 450 m/s, increase in crack density, AE during heating	Some
La Lumbre andesite (M. J. Heap et al., 2017)	Volcán de Colima Mexico	26.5	~2,500 at (1 MPa effective isotropic stress)	Glassy groundmass	Yes (<1.5 mm, 40% of volume)	Yes (<1.5 mm)	Yes (up to a few mm in length)	200, 400, 600, 800, 900°C	No change in porosity, permeability or v_P	No
Dacite (Coats et al., 2018)	Mt Unzen, Japan	10–32	–	Groundmass	Phenocrysts (>3 mm)	Yes (<0.5 mm)	Few	900°C	Little change in porosity or rock strength	No/little
Basalt (Eggertsson et al., 2020)	Krafla volcano, Iceland	10.9–12.1	–	Fine-grained groundmass	Crystals <0.1 mm	Yes (up to ~1 mm)	Few	450°C	Little change in porosity, increase in permeability	Yes
Felsite (Eggertsson et al., 2020)	Krafla volcano, Iceland	9.4–10.3	–	Fine-grained groundmass	Yes (up to several mm)	Few (<0.1 mm)	Highly fractured	450°C	No change in porosity or permeability	No
Altered andesite (Mordensky et al., 2019)	Rotokawa, New Zealand	7.5–18.5	2,200–2,500	Microlitic groundmass	Yes	Yes (up to ~1 mm)	Few (<0.2 mm)	350–739°C	Decrease in v_P, increase in permeability	Yes >400°C
Basalt (M. J. Heap et al., 2009)	Mt Etna, Sicily, Italy	4.80	3,200	Fine-grained groundmass	Yes	Yes	Highly fractured	900°C	No change in elastic moduli	No
Santorini (Daoud et al., 2020)	Santorini	13	4,600	Fine-grained groundmass	Yes	Yes (>0.5 mm)	Yes	900°C	7% reduction in v_P, 98% of AE during cooling	Yes
Basalt (Daoud et al., 2020)	Seljadur, Iceland	4	5,400	Fine-grained groundmass	Yes	Yes	Few	900°C	33% reduction in v_P, 94% of AE during cooling	Yes
Basalt (Malenda & Vanorio, 2023)	Mt Etna, Sicily, Italy	7.49	~4,450	Crystallized	Yes	Some large pores (~10–300 μm)	Yes	350°C, shock cooling	20% reduction in v_P	Yes

Note. Only studies documenting both the physical properties (here, porosity and *P*-wave velocity) and microstructural descriptions were selected. All measurements of v_P—*P*-wave velocity—were made at room temperature.

full-length crystal-boundary cracks (including intracrystalline cracks) from the new nucleation and extension sites formed during heating. As we do not observe a decrease in wave velocity of the three samples during heating (Figure 8), it does not appear that any significant thermal microcracking occurs during the heating stage in the three samples studied herein.

Here, to explain the significant thermal microcracking during cooling in the clearest case of the RCB, we may look to the thermal expansion measurements (Figure 9b). The TEC of the RCB sample with heating during the first cycle shows a strong inflexion and even becomes negative, resulting in a net shortening of the sample over the first cycle (Figure 9b). This shortening is indicative of structural relaxation of the material, which may occur well below the glass transition temperature (Kato et al., 2008). We suggest that, as the rock has deformed during heating to accommodate some thermal stress, the sample is in a new structural state, and cooling tends to instead increase the thermal stress within the rock. The build-up of thermal stress leads ultimately to thermal microcracking toward the end of cooling, as evidenced by the velocity decrease and increased AE rate (Figure 6). We do not observe any indication of stress relaxation during the heating of EB, and an inflection in the TEC data is present for the La Lumbre andesite, but less accentuated than for the RCB (Figure 9). This would explain the lack of significant thermal microcracking during cooling for the EB, and more limited thermal microcracking for the La Lumbre andesite, in comparison with the RCB.

In a study of thermal stress and microcracking during cooling, André et al. (2017) used a two-phase model material in which a borosilicate glass matrix contained spherical beads of alumina. This material model is a good approximation for the RCB and La Lumbre andesite, which have large inclusions (i.e., phenocrysts) within a glassy groundmass (Figure 1). The alumina sample was heated to the temperature of the glass transition (450°C) and then cooled back to room temperature. During cooling, the mismatch in TEC between the matrix and inclusions resulted in microcracking due to a build-up of tensile stress within the matrix. André et al. (2017) then performed numerical simulations using a discrete element model and were able to reproduce the observed thermal microcracking, with the onset of microcracking in the simulation occurring during cooling at 200°C. This study supports our conclusion that thermal microcracking may occur during cooling where the sample is first heated to a temperature where it may experience structural relaxation.

5.3. Velocity Change During Heating and Cooling

The strong increase velocity (of up to 40%; Figure 8) with increasing temperature is opposite to observations made for granite, where wave velocity decreases with increasing temperature during repeated thermal cycling (Griffiths et al., 2018; H. F. Wang et al., 1989). To highlight this difference, Figure 10 shows a summary of the results of Griffiths et al. (2018), for which Westerly Granite followed the same heating and cooling procedure over three cycles, whilst monitoring AE and measuring v_P. Following cycle 1—for which the high AE rate and irreversible velocity change are indicative of thermal microcracking—the AE rate is lower and v_P decreases near reversibly with increasing temperature. This velocity decrease during heating of cycles 2 and 3 points to a widening of microcracks due to the mismatched expansion of grains.

Nevertheless, a velocity increase has been observed when heating basalts. Kern (1982) observed stress relaxation of basalt when heated under a very high confining pressure of 600 MPa, concluding that the porosity within basalts may be closed when heated under high pressures and result in increasing elastic wave velocities. Lebedev et al. (2021) measured a slight increase in *P*-wave velocity of a dry sample basalt when heated to temperatures of up to 700°C under 600 MPa confining pressure. The velocity increase began from around 300°C. Matsushima (1981) measured the v_P and v_S of basic and acidic igneous rocks and volcanic glasses when heated up to 900°C at a constant stress of 1,000–2,000 MPa. The velocity increased with increasing temperature for a glassy andesite (Sanukite) up to about 600°C and decreased at temperatures above 600°C. For basaltic glass, these authors found that the velocity decreased throughout heating (from about 6.84 to 6.64 km/s under 1,050 MPa).

To better understand the change in velocity with temperature, we can look to the mineralogy of the materials (Table 1) and the influence of temperature on the velocity of the main constituents. Here, all samples have between 44% and 50% plagioclase (Table 1). Kono et al. (2008) measured a reversible increase in the v_P of and v_S of plagioclase (An51 ± 1) when heated to and cooled from 700°C under a confining pressure of 1 GPa. As mentioned above, the velocity of andesite glass has been observed to increase with increasing temperature at a pressure of 1,050 MPa (Matsushima, 1981). The La Lumbre andesite contains 42.4% glass (Table 1), which could indeed contribute to the increase in the wave velocity observed during repeated heating cycles (Figure 8).

However, The EB contains no glass and the 32.9% glass in the RCB glass may contribute to a decrease rather than an increase in velocity, as observed by Matsushima (1981) for basalt glass. Note that we do not observe a significant amount of quartz in these samples (<1%, Table 1). In larger quantities, quartz could have a strong influence on the velocity (decrease with increasing temperature), and result in significant thermal microcracking across the alpha-beta phase transition at about 573°C (Glover et al., 1995). In summary, the velocity change of the mineral constituents does not explain the large changes in velocity during heating observed for all samples (Figure 8), and another explanation is required.

As the velocity decrease during heating of the granite is caused by widening of microcracks, we suggest that the increase in velocity during heating for our volcanic rock samples is due to the closure of the microcracks—both pre-existing and generated during the first cycle. As both the TEC and the velocities during cycles 2 and 3 follow the values during cooling of cycle 1, we anticipate that the crack opening during cooling of cycle 1 is almost entirely reversed when heating. We anticipate that the difference in behavior between the two rocks—crack widening versus crack closure—is due to differences between the grain size of the volcanic materials in this study and the grain size of granite, relative to the length of the microcracks they host. For granite, microcracks are most often at the length-scale of the grains and below. Volcanic rock, on the other hand, may consist of an amorphous glassy groundmass or a partially or completely crystallized groundmass (consisting of small crystals called microlites) that may or may not host larger crystals (phenocrysts). Microcracks in volcanic rocks can therefore be many orders of magnitude larger than the size of the crystals through which they pass (as seen in the microstructure of our samples; Figure 1). (We note that other volcanic rocks, such as tuffs, can be granular and may behave differently.) Micromechanical models of thermal stress build-up in granite consider a crack length lower than the grain size (e.g., Fredrich & Wong, 1986), but a better analog for volcanic rock might be a crack within a homogeneous material. One example of such a model is that of Giannopoulos and Anifantis (2005), who demonstrated using 2D finite element modeling how a crack within a homogeneous material may close when the material is heated, in accordance with the observations of this study.

5.4. A Review of Thermal Microcracking Studies on Volcanic Rock

Historically, studies monitoring thermal microcracking have focused on igneous rocks, and in particular granite, observing AE mostly during the heating stage (Griffiths et al., 2018; Todd, 1973; Yong & Wang, 1980), although AE may also be observed during cooling in granite (Griffiths et al., 2018). In granite, the influence of temperature on the thermal expansion of crystals, and the resulting build-up of thermal stresses due to thermal expansion mismatch is well studied and mostly well understood.

In volcanic rock, however, the occurrence of thermal microcracking is highly variable depending on the material. Table 2 gives an overview of studies of thermal microcracking in volcanic rock, including measurements (at ambient pressure and temperature) and information on the: mineralogy; porosity; v_P; the presence and size of phenocrysts; the initial microcrack characteristics; and whether microcracking was observed following thermal stressing. Of these studies, none have measured elastic wave velocities during thermal stressing, and only a few have monitored AE during cooling (Browning et al., 2016; Daoud et al., 2020; M. J. Heap et al., 2014). As such, this table does not distinguish whether microcracking occurred during heating or cooling.

Of the data in Table 2, the reported pore size, presence of pre-existing microcracks, presence of phenocrysts, and nature of the groundmass (completely crystallized vs. partially crystallized) do not have a clear role in determining whether microcracking occurs. However, the initial porosity and v_P appear to correlate with the occurrence of thermal microcracking. Figure 11 shows the initial v_P as a function of porosity for all volcanic rocks listed in Table 2, with symbol type indicating whether the samples underwent significant thermal microcracking when heated and cooled. Where ranges of v_P or porosity values are given for a study, the mid-range value is taken. We see that all volcanic rocks with both v_P greater than 4,000 m/s and porosities less than 10% underwent thermal microcracking. For *P*-wave velocities lower than 4,000 m/s, the correlation between the occurrence of thermal microcracking, v_P, and porosity is less clear (Figure 11).

For the three rocks studied here, the formation of microcracks during the first heating and cooling cycle appears related to whether the sample contains a pre-existing network of microcracks—as suggested in previous studies (e.g., Eggertsson et al., 2020; M. J. Heap et al., 2014; Vinciguerra et al., 2005). The RCB (this study) and the Seljadur basalt of Browning et al. (2016) are comparable in terms of their low porosity and high initial *P*-wave velocities (Table 2), indicating a low crack density prior to heating and greater susceptibility to thermal

microcracking. For these samples, the number of AE hits during cooling is significantly higher than during heating: an indication that thermal microcracks formed during cooling. On the other hand, EB, which has both a low porosity and low *P*-wave velocity owing to its high concentration of microcracks (Figure 11, Table 2), undergoes very little microcracking when heated and cooled (Table 2). This is also true for the low-porosity andesite measured by M. J. Heap, Coats, et al. (2018) (Table 2).

Both the La Lumbre andesite (this study) and the Nea Kameni dacite of Browning et al. (2016) contain large pores and pre-existing microcracks, and represent two of the most porous samples within our compiled data set (Table 2). In both cases, AE activity is observed during the first cycle during both heating and cooling, although mostly during cooling. This suggests that, while most microcracking occurs during cooling, the thermal stresses during heating also results in microcracking. This may be due to a weakened structure of the rock due to the presence of large pores. However, we note that M. J. Heap et al. (2017) found no changes in porosity, *P*-wave velocity, and permeability in a porous andesite (which contains pores and pre-existing microcracks) exposed to 900°C. Whether or not high-porosity rocks, which often contain pores and can also contain microcracks, undergo thermal microcracking may depend on other microstructural parameters not considered here.

We note that for the sample selection of this study, we do not expect transformation of minerals within the studied temperature range (see minerology in Table 1). Mineral transformation has been observed in other volcanic materials to cause mechanical weakening (M. J. Heap et al., 2012; M. J. Heap, Kushnir, et al., 2018) and increase permeability (Mordensky et al., 2019). For example, we note that for basalts containing zeolites, velocity has been seen to decrease significantly when heated to beyond 350°C (Kern, 1982) due to the breakdown of zeolites through their dehydration, resulting in increase in microcrack porosity. In this case, significant thermal microcracking is expected during the heating phase. Such behavior—which may also occur for rocks containing chlorites or clays (Kern, 1982)—was not observed for our rocks due to their absence of these minerals, but should be accounted for when relevant.

5.5. The Consequence of Temperature Change on the Mechanical and Flow Properties of Volcanic Rock

Extrapolating from room temperature measurements made on thermally-microcracked rock (Darot et al., 1992; C. David et al., 1999; E. C. David et al., 2012; Griffiths et al., 2017), we anticipate that the formation of microcracks and their opening and closing may have significant effects on a range of properties including permeability and strength. In the rare instances where changes in physical and mechanical properties of volcanic rock have been measured at high temperatures, measurements do indeed align with the hypothesis of microcrack closure with increasing temperature. Coats et al. (2018) tested the strength of dome rocks from Mt. Unzen volcano at ambient temperature both before and following heating to 900°C, and at 900°C. The authors found that heating the samples to 900°C and cooling had no effect on their strength under ambient temperature conditions, but when deformed in the brittle regime (at a strain rate of 1×10^{-3} s) at 900°C, the samples were stronger. M. J. Heap, Coats, et al. (2018) followed a similar procedure to Coats et al. (2018) but on andesitic dome rock from Volcán de Colima. M. J. Heap, Coats, et al. (2018) attributed the increase in strength, and Young's modulus, with increasing temperature to the closure of microcracks. These authors also found that all thermal stressing scenarios (even quench-cooling) resulted in no change in rock strength at room temperature, although the rock was stronger when deformed at temperatures ranging from 400 to 700°C. Meredith and Atkinson (1985) measured an increase in the fracture toughness of a gabbro with increasing temperature; and Duclos and Paquet (1991) showed the compressive strength of basalt to increase from ∼340 MPa at ambient temperature to ∼450 MPa at 650°C. Gaunt et al. (2016) measured a decrease in the permeability of a dacite by more than four orders of magnitude when heated to 800°C, which was suggested to be caused by crack closure. Kushnir et al. (2017) attributed a decrease in the permeability of basaltic andesites above the glass transition as due to relaxation and crack closure. Through our multi-physical approach, we can more confidently link the previously observed increase in the strength of volcanic rock at high temperature to microcrack closure and, importantly, we show that this phenomenon may be expected even at low confining pressures.

We interpret the results of our experiments as evidence of crack closure with increasing temperature, at temperatures well below the glass transition where we might expect significant stress relaxation, as well as in volcanic rock containing no glass. Whilst the physical properties of some volcanic rocks have shown little permanent change following cyclic thermal stressing (e.g., M. J. Heap et al., 2014; M. J. Heap, Coats, et al., 2018; Kendrick et al., 2013; Schaefer et al., 2015)—indicating that the rock was already highly microcracked—we expect that

some of the pre-existing microcracks will close at higher temperatures and influence rock physical properties (i.e., an increase in strength, Young's modulus, and a decrease in permeability).

Whilst our samples were unconfined in our experiments, we may expect wave velocities to increase with temperature even at depth. Kern (1982) observed stress relaxation of basalt when heated under a very high confining pressure of 600 MPa, concluding that the porosity within basalts may be closed when heated under high pressures and result in increasing elastic wave velocities. In contrast to our measurements, Kern (1982) measured a negative sample elongation with increasing temperature, that is, a bulk contraction of the rock during heating associated with a reduction in porosity. We expect that the low aspect ratio microcracks are the easiest to close at low stresses (as in this study) and higher aspect ratio voids may also close at higher stress (similar to Kern (1982)). In experiments by Fortin et al. (2011), Stanchits et al. (2006), and Vinciguerra et al. (2005), the elastic wave velocities of basalt from Mt. Etna were shown to continually increase with confining pressure (up to 190 MPa in the study by Fortin et al. (2011)), indicating that some high aspect ratio microcracks remained open throughout. Scheu et al. (2006) measured an increase in the v_P of a dacite from Mt. Unzen volcano from 5.11–5.48 to 5.51–5.73 km/s when heated to 600°C under 100 MPa confining pressure, indicating that a velocity increase with temperature, as observed here, can also be expected at depth. The diversity of microcrack populations in terms of their geometry and propensity to closure at certain stresses and temperatures means that even at high pressure, some microcracks still remain open that can be closed by additional thermal or mechanical stresses.

We also note that our experiments were performed on dry samples, and that fluid saturation may influence the velocity change with temperature. Jaya et al. (2010) took water-saturated samples of basalt and hyaloclastite recovered from wells within alteration zones of the Krafla and Hengill geothermal fields, respectively, and measured *P*-wave velocity whilst heating them to temperatures of up to 250°C within a triaxial cell. These authors measured a decrease in the velocity with increasing temperature, attributed to the formation of bubbles in the pore fluid and thermal microcracks. These results are contrary to the results of this study, on dry samples, in which velocity is seen to increase within increasing temperature. The experiments of Jaya et al. (2010) suggest that, for temperatures of up to 250°C, water saturation may play a significant role on the evolution of velocity with temperature.

5.6. Field-Scale Implications for Thermal Stressing of Volcanic Rock

5.6.1. Volcanic Environments

The influence of temperature on the seismic velocity of volcanic rock is of critical importance for geophysical monitoring of volcanoes. Temporal changes in seismic velocity may be linked to a number of factors, including changes in confining pressure, pore fluid pressure, fluid saturation, and fluid viscosity, as well as temperature, porosity and crack density of the host rock (Sanders et al., 1995). Seismic monitoring is used to infer changes in the structure of volcanoes, for example, at: Mt. Etna (Brenguier et al., 2007; De Luca et al., 1997; Laigle et al., 2000; Patanè et al., 2002; Villaseñor et al., 1998); Mt. Erebus volcano, Antarctica (Grêt, 2005); Merapi volcano (Sens-Schönfelder & Wegler, 2006). For example, at Volcán de Colima (from which the La Lumbre andesite originates), Lamb et al. (2017) used coda wave interferometry of ambient seismic noise to observe an apparent decrease in wave velocity of 0.2% prior to eruption. The velocity decrease was anticipated to be due to fracture formation within the volcano as magma rose. The significant velocity changes with temperature observed in this study (Figure 8) may rival changes in velocity due to the mechanical deformation in volcanic environments. For example, an increase in v_P and v_S of basalt from Mt. Etna as a function of increasing confining pressure was observed by Fortin et al. (2011), from 3.1 km/s at room pressure to 5.5 km/s at 190 MPa; a velocity change of the same order of magnitude as those observed in this study.

Crack density also affects the permeability of volcanic rock, which can ultimately contribute to whether or not gas may escape, a factor dictating the eruptive behavior of a volcano (Eichelberger et al., 1986; Farquharson et al., 2017; M. J. Heap et al., 2019; Melnik et al., 2005; Sparks et al., 1997). Further, as microcracks influence the mechanical properties of rock, the influence of temperature on the geomechanics of volcanoes has implications for magma ascent and the stability of the volcanic edifice (Coats et al., 2018; M. J. Heap & Violay, 2021).

Here, we observed a thermal Kaiser stress-memory effect over multiple thermal stressing cycles of the volcanic rock samples, which resulted in very limited thermal microcracking during repeated cycles (Figures 5–7). The Kaiser effect has previously been observed at the scale of the volcano by Heimisson et al. (2015), who observed

cyclic inflation and deflation at the surface of due to magma flow within Krafla volcano, and which only resulted in seismicity once the maximum inflation of the previous cycles was surpassed. This suggests that cyclic thermal stressing associated with the movement of magma may also produce a Kaiser effect on a larger scale, whereby thermal stressing of the surrounding rock mass may only result in cracking once the rock reaches temperatures greater (or lower) than those already experienced.

5.6.2. Geothermal Reservoirs

Geothermal reservoirs are often hosted in volcanic rock (Bertani, 2016; Grant, 2013), for example,: the Ethiopian Rift valley (Teklemariam et al., 2000), which exploits the upflow of geothermal fluids through basaltic lavas (Battistelli et al., 2002); sites in New Zealand such as the Rotokawa reservoir within andesitic rock (McNamara et al., 2015; Siratovich et al., 2014); and the basaltic Krafla and Námafjall geothermal sites in Iceland (Björnsson et al., 1977; Thór Gudmundsson & Arnórsson, 2002). Volcanic reservoirs may even host very high-temperature geothermal systems within which supercritical conditions may be reached (for pure water, $T > 374$°C, $P > 22.1$ MPa, for seawater, $T > 406$°C, $P > 29.8$ MPa), offering new potential for exploiting very high enthalpy fluids (Reinsch et al., 2017).

When injecting cool fluids into such reservoirs, temperature changes may influence rock properties including elastic wave velocities (Figures 5–7) and, through seismic monitoring, provide valuable information on changes within a reservoir due to fluid circulation (Calò et al., 2011; Lehujeur et al., 2017, 2018; Obermann et al., 2015; Richter et al., 2014). As for volcanoes, it is important to understand the influence of temperature on wave velocity to infer temperature changes within the reservoir and distinguish them from changes due to fluid pressure and other mechanical stresses.

Injectivity at the injection well is a key parameter for geothermal reservoirs. In geothermal systems, changes in temperature and the resulting thermal stresses may increase well injectivity through fracturing (Eggertsson et al., 2020; Grant et al., 2013; Huenges et al., 2013; Jansen & Miller, 2017; Siratovich et al., 2011), but may also negatively impact well stability (Bérard & Cornet, 2003). Our results suggest that temperature changes due to injection and production may result in crack opening, ultimately reducing the strength and stiffness of the host rock.

6. Conclusions

Samples of Rubble Creek and Etna basalts (~1% and ~4% porosity, respectively) and the La Lumbre andesite (~23% porosity) were heated and cooled over three cycles: to temperatures of 450°C whilst measuring v_P and monitoring AEs; and to temperatures of 700°C whilst measuring sample elongation.

During heating and cooling cycles 2 and 3, both v_P and the sample lengths increased reversibly with increasing temperature. We conclude that the significant increase in v_P measured during heating (of up to about 40%)—which is opposite to observations made for granite—is due to closure of microcracks with increasing temperature.

During the first cycle, we observed a higher rate of detected AE and an irreversible decrease in v_P, indicating significant microcracking in the RCB and some microcracking in the La Lumbre andesite. Additionally, for both the RCB and La Lumbre andesite, we observed inflections in the TEC during heating, indicative of structural relaxation. We anticipate that the subsequent cooling of the restructured material leads to an accumulation of thermal stress and ultimately microcracking during the cooling phase. In contrast, the EB, characterized by a high density of pre-existing microcracks but low porosity, exhibited a quasi-reversible increase in v_P with increasing temperature throughout all cycles. Notably, we did not observe inflections in TEC, and the AE activity remained low, indicating minimal microcracking in this sample.

For comparison with our experimental results, we compiled data from previous experimental studies of thermal stressing of volcanic rocks and conclude that rocks with low porosity and low initial crack densities are particularly susceptible to thermal microcracking. Our results and review of the literature highlight the influence of the initial microstructure and thermal stress history on the occurrence of thermal microcracking within volcanic rock.

We anticipate that, owing to the contribution of microcrack closure, the influence of temperature on the physical, mechanical and transport properties of volcanic rock may be greater than previously understood, having strong implications for the behavior and monitoring of volcanic and geothermal systems at all depths.

Data Availability Statement

The data files used in this paper are available at Griffiths et al. (2024).

Acknowledgments

This work of the Interdisciplinary Thematic Institute GeoT, as part of the ITI 2021–2028 program of the University of Strasbourg, CNRS and Inserm, was supported by IdEx Unistra (ANR-10-IDEX-0002), and by SFRI-STRAT'US project (ANR-20-SFRI-0012) under the framework of the French Investments for the Future Program. This work was also supported by the framework of LABEX Grant ANR-11-LABX-0050_G-EAU-THERMIE-PROFONDE and therefore benefits from state funding managed by the Agence Nationale de la Recherche (ANR) as part of the "Investissements d'avenir" program. The authors would like to thank Bertrand Renaudie for sample preparation, Alain Steyer and Laurent Rihouey for their help with the construction of the experimental setup, and Jamie Farquharson and Alex Kushnir for experimental support. Michael Heap acknowledges support from the Institut Universitaire de France (IUF). Kelly Russell, Sergio Vinciguerra, and Nick Varley are thanked for their help sourcing the materials used in this study. The comments of two reviewers and the editor helped improved this manuscript.

References

Abbott, J., Abdullin, S., Abbiendi, G., & Guéguen, Y. (2006). Acoustic emission and velocities associated with the formation of compaction bands in sandstone. *Journal of Geophysical Research*, *111*(B10), B10203. https://doi.org/10.1029/2005JB003854

Aker, E., Kühn, D., Vavryčuk, V., Soldal, M., & Oye, V. (2014). Experimental investigation of acoustic emissions and their moment tensors in rock during failure. *International Journal of Rock Mechanics and Mining Sciences*, *70*, 286–295. https://doi.org/10.1016/j.ijrmms.2014.05.003

André, D., Levraut, B., Tessier-Doyen, N., & Huger, M. (2017). A discrete element thermo-mechanical modelling of diffuse damage induced by thermal expansion mismatch of two-phase materials. *Computer Methods in Applied Mechanics and Engineering*, *318*, 898–916. https://doi.org/10.1016/j.cma.2017.01.029

Atkinson, B. K., MacDonald, D., & Meredith, P. G. (1984). Acoustic response and fracture mechanics of granite subjected to thermal and stress cycling experiments. In *Serail Rock soil mechanics; (United States), 8*. Retrieved from https://www.osti.gov/scitech/biblio/7064265

Battistelli, A., Yiheyis, A., Calore, C., Ferragina, C., & Abatneh, W. (2002). Reservoir engineering assessment of Dubti geothermal field, northern Tendaho Rift, Ethiopia. *Geothermics*, *31*(3), 381–406. https://doi.org/10.1016/S0375-6505(01)00039-6

Baud, P., Klein, E., & Wong, T. (2004). Compaction localization in porous sandstones: Spatial evolution of damage and acoustic emission activity. *Journal of Structural Geology*, *26*(4), 603–624. https://doi.org/10.1016/j.jsg.2003.09.002

Bauer, S. J., & Handin, J. (1983). Thermal expansion and cracking of three confined water-saturated igneous rocks to 800°C. *Rock Mechanics and Rock Engineering*, *16*(3), 181–198. https://doi.org/10.1007/bf01033279

Bérard, T., & Cornet, F. H. (2003). Evidence of thermally induced borehole elongation: A case study at Soultz, France. *International Journal of Rock Mechanics and Mining Sciences*, *40*(7–8), 1121–1140. https://doi.org/10.1016/S1365-1609(03)00118-7

Bertani, R. (2016). Geothermal power generation in the world 2010–2014 update report. *Geothermics*, *60*, 31–43. https://doi.org/10.1016/j.geothermics.2015.11.003

Björnsson, A., Saemundsson, K., Einarsson, P., Tryggvason, E., & Grönvold, K. (1977). Current rifting episode in north Iceland. *Nature*, *266*(5600), 318–323. https://doi.org/10.1038/266318a0

Bonaccorso, A., Calvari, S., Coltelli, M., Del Negro, C., & Falsaperla, S. (2004). Mt. Etna: Volcano laboratory. In *Washington DC American geophysical union geophysical monograph series* (Vol. 143).

Brenguier, F., Shapiro, N. M., Campillo, M., Nercessian, A., & Ferrazzini, V. (2007). 3-D surface wave tomography of the Piton de la Fournaise volcano using seismic noise correlations. *Geophysical Research Letters*, *34*(2), 2305. https://doi.org/10.1029/2006gl028586

Browning, J., Meredith, P., & Gudmundsson, A. (2016). Cooling-dominated cracking in thermally stressed volcanic rocks. *Geophysical Research Letters*, *43*(16), 8425. https://doi.org/10.1002/2016GL070532

Calò, M., Dorbath, C., Cornet, F. H., & Cuenot, N. (2011). Large-scale aseismic motion identified through 4-D P-wave tomography: Temporal subsetting of the stimulation period. *Geophysical Journal International*, *186*(3), 1295–1314. https://doi.org/10.1111/j.1365-246X.2011.05108.x

Cengel, Y., & Ghajar, A. (2010). Heat and mass transfer: Fundamentals and applications (pp. 217–284).

Coats, R., Kendrick, J. E., Wallace, P. A., Miwa, T., Hornby, A. J., Ashworth, J. D., et al. (2018). Failure criteria for porous dome rocks and lavas: A study of Mt. Unzen, Japan. *Solid Earth*, *9*(6), 1299–1328. https://doi.org/10.5194/se-9-1299-2018

Cooper, H. W., & Simmons, G. (1977). The effect of cracks on the thermal expansion of rocks. *Earth and Planetary Science Letters*, *36*(3), 404–412. https://doi.org/10.1016/0012-821X(77)90065-6

Daoud, A., Browning, J., Meredith, P. G., & Mitchell, T. M. (2020). Microstructural controls on thermal crack damage and the presence of a temperature-memory effect during cyclic thermal stressing of rocks. *Geophysical Research Letters*, *47*(19), e2020GL088693. https://doi.org/10.1029/2020GL088693

Darot, M., Gueguen, Y., & Baratin, M.-L. (1992). Permeability of thermally cracked granite. *Geophysical Research Letters*, *19*(9), 869–872. https://doi.org/10.1029/92GL00579

David, C., Menendez, B., & Darot, M. (1999). Influence of stress-induced and thermal cracking on physical properties and microstructure of La Peyratte granite. *International Journal of Rock Mechanics and Mining Sciences*, *36*(4), 433–448. https://doi.org/10.1016/s0148-9062(99)00010-8

David, E. C., Brantut, N., Schubnel, A., & Zimmerman, R. W. (2012). Sliding crack model for nonlinearity and hysteresis in the uniaxial stress-strain curve of rock. *International Journal of Rock Mechanics and Mining Sciences*, *52*, 9–17. https://doi.org/10.1016/j.ijrmms.2012.02.001

De Luca, G., Filippi, L., Patanè, G., Scarpa, R., & Vinciguerra, S. (1997). Three-dimensional velocity structure and seismicity of Mt. Etna Volcano, Italy. *Journal of Volcanology and Geothermal Research*, *79*(1), 123–138. https://doi.org/10.1016/S0377-0273(97)00026-7

Doebelin, N., & Kleeberg, R. (2015). Profex: A graphical user interface for the Rietveld refinement program BGMN. *Journal of Applied Crystallography*, *48*(5), 1573–1580. https://doi.org/10.1107/s1600576715014685

Duclos, R., & Paquet, J. (1991). High-temperature behaviour of basalts—Role of temperature and strain rate on compressive strength and Kic toughness of partially glassy basalts at atmospheric pressure. In *International journal of rock mechanics and mining sciences and geomechanics abstracts* (Vol. 28, pp. 71–76). Elsevier.

Eggertsson, G. H., Lavallée, Y., Kendrick, J. E., & Markússon, S. H. (2020). Improving fluid flow in geothermal reservoirs by thermal and mechanical stimulation: The case of Krafla volcano, Iceland. *Journal of Volcanology and Geothermal Research*, *391*, 106351. https://doi.org/10.1016/j.jvolgeores.2018.04.008

Eichelberger, J. C., Carrigan, C. R., Westrich, H. R., & Price, R. H. (1986). Non-explosive silicic volcanism. *Nature*, *323*(6089), 598–602. https://doi.org/10.1038/323598a0

Faletti, D. W., & Ethridge, L. J. (1988). A method for predicting cracking in waste glass canisters. *Nuclear & Chemical Waste Management*, *8*(2), 123–133. https://doi.org/10.1016/0191-815x(88)90071-x

Farquharson, J. I., Baud, P., & Heap, M. J. (2017). Inelastic compaction and permeability evolution in volcanic rock. *Solid Earth*, *8*(2), 561–581. https://doi.org/10.5194/se-8-561-2017

Fortin, J., Stanchits, S., Dresen, G., & Guéguen, Y. (2006). Acoustic emission and velocities associated with the formation of compaction bands in sandstone. *Journal of Geophysical Research*, *111*(B10), B10203. https://doi.org/10.1029/2005jb003854

Fortin, J., Stanchits, S., Vinciguerra, S., & Guéguen, Y. (2011). Influence of thermal and mechanical cracks on permeability and elastic wave velocities in a basalt from Mt. Etna volcano subjected to elevated pressure. *Tectonophysics*, *503*(1), 60–74. https://doi.org/10.1016/j.tecto.2010.09.028

Fredrich, J. T., & Wong, T. (1986). Micromechanics of thermally induced cracking in three crustal rocks. *Journal of Geophysical Research*, *91*(B12), 12743. https://doi.org/10.1029/JB091iB12p12743

Gaunt, H. E., Sammonds, P. R., Meredith, P. G., & Chadderton, A. (2016). Effect of temperature on the permeability of lava dome rocks from the 2004–2008 eruption of Mount St. Helens. *Bulletin of Volcanology*, *78*(4), 30. https://doi.org/10.1007/s00445-016-1024-5

Giannopoulos, G. I., & Anifantis, N. K. (2005). Finite element analysis of crack closure in two-dimensional bodies subjected to heating. *Computers & Structures*, *83*(4–5), 303–314. https://doi.org/10.1016/j.compstruc.2004.10.008

Glover, P. W. J., Baud, P., Darot, M., Meredith, P. G., Boon, S. A., LeRavalec, M., et al. (1995). Alpha/beta phase transitions in quartz monitored using acoustic emissions. *Geophysical Journal International*, *120*(3), 775–782. https://doi.org/10.1111/j.1365-246x.1995.tb01852.x

Grant, M. A. (2013). *Geothermal reservoir engineering*. Elsevier.

Grant, M. A., Clearwater, J., Quinao, J., Bixley, P. F., & Le Brun, M. (2013). Thermal stimulation of geothermal wells: A review of field data. In *Thirty-eighth workshop on geothermal reservoir engineering*.

Grêt, A., Snieder, R., Aster, R. C., & Kyle, P. R. (2005). Monitoring rapid temporal change in a volcano with coda wave interferometry. *Geophysical Research Letters*, *32*(6), L06304. https://doi.org/10.1029/2004GL021143

Griffiths, L., Dautriat, J., Vera Rodriguez, I., Iranpour, K., Sauvin, G., Park, J., et al. (2019). Inferring microseismic source mechanisms and in situ stresses during triaxial deformation of a North-Sea-analogue sandstone. *Advances in Geosciences*, *49*, 85–93. https://doi.org/10.5194/adgeo-49-85-2019

Griffiths, L., Heap, M. J., Baud, P., & Schmittbuhl, J. (2017). Quantification of microcrack characteristics and implications for stiffness and strength of granite. *International Journal of Rock Mechanics and Mining Sciences*, *100*, 138–150. https://doi.org/10.1016/j.ijrmms.2017.10.013

Griffiths, L., Heap, M. J., Lengliné, O., Baud, P., & Schmittbuhl, J. (2024). Dataset for "thermal stressing of volcanic rock: Microcracking and crack closure monitored through acoustic emission, ultrasonic velocity, and thermal expansion" [Dataset]. Figshare. https://doi.org/10.6084/m9.figshare.24053064

Griffiths, L., Lengliné, O., Heap, M. J., Baud, P., & Schmittbuhl, J. (2018). Thermal cracking in westerly granite monitored using direct wave velocity, coda wave interferometry, and acoustic emissions. *Journal of Geophysical Research: Solid Earth*, *123*(3), 2246–2261. https://doi.org/10.1002/2017JB015191

Hall, K., & Thorn, C. E. (2014). Thermal fatigue and thermal shock in bedrock: An attempt to unravel the geomorphic processes and products. *Geomorphology*, *206*, 1–13. https://doi.org/10.1016/j.geomorph.2013.09.022

Heap, M., Kushnir, A., Griffiths, L., Wadsworth, F., Marmoni, G. M., Fiorucci, M., et al. (2018). Fire resistance of the Mt. Epomeo green tuff, a widely-used building stone on Ischia Island (Italy). *Volcanica*, *1*(1), 33–48. https://doi.org/10.30909/vol.01.01.3348

Heap, M. J., Coats, R., Chen, C., Varley, N., Lavallée, Y., Kendrick, J., et al. (2018). Thermal resilience of microcracked andesitic dome rocks. *Journal of Volcanology and Geothermal Research*, *367*, 20–30. https://doi.org/10.1016/j.jvolgeores.2018.10.021

Heap, M. J., Kushnir, A. R., Vasseur, J., Wadsworth, F. B., Harlé, P., Baud, P., et al. (2020). The thermal properties of porous andesite. *Journal of Volcanology and Geothermal Research*, *398*, 106901. https://doi.org/10.1016/j.jvolgeores.2020.106901

Heap, M. J., Lavallée, Y., Laumann, A., Hess, K. U., Meredith, P. G., & Dingwell, D. B. (2012). How tough is tuff in the event of fire? *Geology*, *40*(4), 311–314. https://doi.org/10.1130/G32940.1

Heap, M. J., Lavallée, Y., Laumann, A., Hess, K. U., Meredith, P. G., Dingwell, D. B., et al. (2013). The influence of thermal-stressing (up to 1000°C) on the physical, mechanical, and chemical properties of siliceous-aggregate, high-strength concrete. *Construction and Building Materials*, *42*, 248–265. https://doi.org/10.1016/j.conbuildmat.2013.01.020

Heap, M. J., Lavallée, Y., Petrakova, L., Baud, P., Reuschlé, T., Varley, N. R., & Dingwell, D. B. (2014). Microstructural controls on the physical and mechanical properties of edifice-forming Andesites at Volcán de Colima, Mexico. *Journal of Geophysical Research: Solid Earth*, *119*(4), 2963. https://doi.org/10.1002/2013JB010521

Heap, M. J., Troll, V. R., Kushnir, A. R., Gilg, H. A., Collinson, A. S., Deegan, F. M., et al. (2019). Hydrothermal alteration of andesitic lava domes can lead to explosive volcanic behaviour. *Nature Communications*, *10*(1), 1–10. https://doi.org/10.1038/s41467-019-13102-8

Heap, M. J., Vinciguerra, S., & Meredith, P. G. (2009). The evolution of elastic moduli with increasing crack damage during cyclic stressing of a basalt from Mt. Etna volcano. *Tectonophysics*, *471*(1–2), 153–160. https://doi.org/10.1016/j.tecto.2008.10.004

Heap, M. J., Violay, M., Wadsworth, F. B., & Vasseur, J. (2017). From rock to magma and back again: The evolution of temperature and deformation mechanism in conduit margin zones. *Earth and Planetary Science Letters*, *463*, 92–100. https://doi.org/10.1016/j.epsl.2017.01.021

Heap, M. J., & Violay, M. E. (2021). The mechanical behaviour and failure modes of volcanic rocks: A review. *Bulletin of Volcanology*, *83*(5), 1–47. https://doi.org/10.1007/s00445-021-01447-2

Heimisson, E. R., Einarsson, P., Sigmundsson, F., & Brandsdóttir, B. (2015). Kilometer-scale Kaiser effect identified in Krafla volcano, Iceland: Large-scale Kaiser effect. *Geophysical Research Letters*, *42*(19), 7958–7965. https://doi.org/10.1002/2015GL065680

Hodgkinson, D. P., Lever, D. A., & Rae, J. (1983). Thermal aspects of radioactive waste burial in hard rock. *Progress in Nuclear Energy*, *11*(2), 183–218. https://doi.org/10.1016/0149-1970(83)90019-7

Homand-Etienne, F., & Houpert, R. (1989). Thermally induced microcracking in granites: Characterization and analysis. *International Journal of Rock Mechanics and Mining Sciences & Geomechanics Abstracts*, *26*(2), 125–134. https://doi.org/10.1016/0148-9062(89)90001-6

Huenges, E., Kohl, T., Kolditz, O., Bremer, J., Scheck-Wenderoth, M., & Vienken, T. (2013). Geothermal energy systems: Research perspective for domestic energy provision. *Environmental Earth Sciences*, *70*(8), 3927–3933. https://doi.org/10.1007/s12665-013-2881-2

Isaka, B. A. L., Ranjith, P. G., Rathnaweera, T. D., Perera, M. S. A., & De Silva, V. R. S. (2019). Quantification of thermally-induced microcracks in granite using X-ray CT imaging and analysis. *Geothermics*, *81*, 152–167. https://doi.org/10.1016/j.geothermics.2019.04.007

Jansen, G., & Miller, S. A. (2017). On the role of thermal stresses during hydraulic stimulation of geothermal reservoirs. *Geofluids*, *2017*, 1–15. https://doi.org/10.1155/2017/4653278

Jaya, M. S., Shapiro, S. A., Kristinsdóttir, L. H., Bruhn, D., Milsch, H., & Spangenberg, E. (2010). Temperature dependence of seismic properties in geothermal rocks at reservoir conditions. *Geothermics*, *39*(1), 115–123. https://doi.org/10.1016/j.geothermics.2009.12.002

Jones, C., Keaney, G., Meredith, P., & Murrell, S. (1997). Acoustic emission and fluid permeability measurements on thermally cracked rocks. *Physics and Chemistry of the Earth*, *22*(1), 13–17. https://doi.org/10.1016/S0079-1946(97)00071-2

Kaiser, J. (1953). Erkenntnisse und Folgerungen aus der Messung von Geräuschen bei Zugbeanspruchung von metallischen Werkstoffen. *Archiv für das Eisenhuttenwesen*, *24*(1–2), 43–45. https://doi.org/10.1002/srin.195301381

Kato, H., Chen, H.-S., & Inoue, A. (2008). Relationship between thermal expansion coefficient and glass transition temperature in metallic glasses. *Scripta Materialia*, *58*(12), 1106–1109. https://doi.org/10.1016/j.scriptamat.2008.02.006

Kendrick, J. E., Smith, R., Sammonds, P., Meredith, P. G., Dainty, M., & Pallister, J. S. (2013). The influence of thermal and cyclic stressing on the strength of rocks from Mount St. Helens, Washington. *Bulletin of Volcanology*, *75*(7), 728. https://doi.org/10.1007/s00445-013-0728-z

Kern, H. (1982). Elastic-wave velocity in crustal and mantle rocks at high pressure and temperature: The role of the high-low quartz transition and of dehydration reactions. *Physics of the Earth and Planetary Interiors*, *29*(1), 12–23. https://doi.org/10.1016/0031-9201(82)90133-9

Kolditz, O., Jakobs, L. A., Huenges, E., & Kohl, T. (2013). *Geothermal energy: A glimpse at the state of the field and an introduction to the journal*. Springer.

Kono, Y., Miyake, A., Ishikawa, M., & Arima, M. (2008). Temperature derivatives of elastic wave velocities in plagioclase (An51 1) above and below the order-disorder transition temperature. *American Mineralogist*, *93*(4), 558–564. https://doi.org/10.2138/am.2008.2591

Kushnir, A. R. L., Martel, C., Bourdier, J.-L., Heap, M. J., Reuschlé, T., Erdmann, S., et al. (2016). Probing permeability and microstructure: Unravelling the role of a low-permeability dome on the explosivity of Merapi (Indonesia). *Journal of Volcanology and Geothermal Research*, *316*, 56–71. https://doi.org/10.1016/j.jvolgeores.2016.02.012

Kushnir, A. R. L., Martel, C., Champallier, R., & Wadsworth, F. B. (2017). Permeability evolution in variably glassy basaltic andesites measured under magmatic conditions. *Geophysical Research Letters*, *44*(20), 10. https://doi.org/10.1002/2017gl074042

Laigle, M., Hirn, A., Sapin, M., Lépine, J.-C., Diaz, J., Gallart, J., & Nicolich, R. (2000). Mount Etna dense array local earthquake P and S tomography and implications for volcanic plumbing. *Journal of Geophysical Research*, *105*(B9), 21633–21646. https://doi.org/10.1029/2000JB900190

Lamb, O. D., De Angelis, S., Wall, R. J., Lamur, A., Varley, N. R., Reyes-Dávila, G., et al. (2017). Seismic and experimental insights into eruption precursors at Volcán de Colima. *Geophysical Research Letters*, *44*(12), 6100. https://doi.org/10.1002/2017GL073350

Lebedev, E. B., Kern, H., Pavlenkova, N. I., Lukanin, O. A., Lobanov, K. V., Zharikov, A. V., & Popp, T. (2021). Compressional wave velocity measurements on mafic–ultramafic rocks under high aqueous fluid pressure and temperature help to explain low-velocity zones in the lithosphere. *Scientific Reports*, *11*(1), 13424. https://doi.org/10.1038/s41598-021-92248-2

Lehujeur, M., Vergne, J., Maggi, A., & Schmittbuhl, J. (2017). Ambient noise tomography with non-uniform noise sources and low aperture networks: Case study of deep geothermal reservoirs in northern Alsace, France. *Geophysical Journal International*, *208*(1), 193–210. https://doi.org/10.1093/gji/ggw373

Lehujeur, M., Vergne, J., Schmittbuhl, J., Zigone, D., Le Chenadec, A., & Team, E. (2018). Reservoir imaging using ambient noise correlation from a dense seismic network. *Journal of Geophysical Research: Solid Earth*, *123*(8), 6671–6686. https://doi.org/10.1029/2018jb015440

Li, Z., Fortin, J., Nicolas, A., Deldicque, D., & Guéguen, Y. (2019). Physical and mechanical properties of thermally cracked andesite under pressure. *Rock Mechanics and Rock Engineering*, *52*(10), 3509–3529. https://doi.org/10.1007/s00603-019-01785-w

Lockner, D. (1993). The role of acoustic emission in the study of rock fracture. *International Journal of Rock Mechanics and Mining Sciences & Geomechanics Abstracts*, *30*(7), 883–899. https://doi.org/10.1016/0148-9062(93)90041-B

Malenda, M., & Vanorio, T. (2023). Using acoustic velocities and microimaging to probe microstructural changes caused by thermal shocking of tight rocks. *Frontiers in Earth Science*, *10*, 1054469. https://doi.org/10.3389/feart.2022.1054469

Matsushima, S. (1981). Compressional and shear wave velocities of igneous rocks and volcanic glasses to 900°C and 20 kbar. *Tectonophysics*, *75*(3–4), 257–271. https://doi.org/10.1016/0040-1951(81)90277-8

McNamara, D. D., Massiot, C., Lewis, B., & Wallis, I. C. (2015). Heterogeneity of structure and stress in the Rotokawa geothermal field, New Zealand. *Journal of Geophysical Research: Solid Earth*, *120*(2), 1262. https://doi.org/10.1002/2014JB011480

Melnik, O., Barmin, A. A., & Sparks, R. S. J. (2005). Dynamics of magma flow inside volcanic conduits with bubble overpressure buildup and gas loss through permeable magma. *Journal of Volcanology and Geothermal Research*, *143*(1–3), 53–68. https://doi.org/10.1016/j.jvolgeores.2004.09.010

Meredith, P. G., & Atkinson, B. K. (1985). Fracture toughness and subcritical crack growth during high-temperature tensile deformation of Westerly granite and Black gabbro. *Physics of the Earth and Planetary Interiors*, *39*(1), 33–51. https://doi.org/10.1016/0031-9201(85)90113-X

Meredith, P. G., Knight, K. S., Boon, S. A., & Wood, I. G. (2001). The microscopic origin of thermal cracking in rocks: An investigation by simultaneous time-of-flight neutron diffraction and acoustic emission monitoring. *Geophysical Research Letters*, *28*(10), 2105–2108. https://doi.org/10.1029/2000GL012470

Meredith, P. G., Main, I. G., Clint, O. C., & Li, L. (2012). On the threshold of flow in a tight natural rock. *Geophysical Research Letters*, *39*(4), L04307. https://doi.org/10.1029/2011GL050649

Mordensky, S. P., Kennedy, B. M., Villeneuve, M. C., Lavallée, Y., Reichow, M. K., Wallace, P. A., et al. (2019). Increasing the permeability of hydrothermally altered andesite by transitory heating. *Geochemistry, Geophysics, Geosystems*, *20*(11), 5251–5269. https://doi.org/10.1029/2019GC008409

Nara, Y., Meredith, P. G., Yoneda, T., & Kaneko, K. (2011). Influence of macro-fractures and micro-fractures on permeability and elastic wave velocities in basalt at elevated pressure. *Tectonophysics*, *503*(1–2), 52–59. https://doi.org/10.1016/j.tecto.2010.09.027

Obermann, A., Kraft, T., Larose, E., & Wiemer, S. (2015). Potential of ambient seismic noise techniques to monitor the St. Gallen geothermal site (Switzerland): Monitoring the St. Gallen Geothermal Site. *Journal of Geophysical Research: Solid Earth*, *120*(6), 4301–4316. https://doi.org/10.1002/2014JB011817

O'Connell, R. J., & Budiansky, B. (1974). Seismic velocities in dry and saturated cracked solids. *Journal of Geophysical Research*, *79*(35), 5412–5426. https://doi.org/10.1029/JB079i035p05412

Patanè, D., Chiarabba, C., Cocina, O., De Gori, P., Moretti, M., & Boschi, E. (2002). Tomographic images and 3D earthquake locations of the seismic swarm preceding the 2001 Mt. Etna eruption: Evidence for a dyke intrusion. *Geophysical Research Letters*, *29*(10), 135-1. https://doi.org/10.1029/2001GL014391

Reinsch, T., Dobson, P., Asanuma, H., Huenges, E., Poletto, F., & Sanjuan, B. (2017). Utilizing supercritical geothermal systems: A review of past ventures and ongoing research activities. *Geothermal Energy*, *5*(1), 1–25. https://doi.org/10.1186/s40517-017-0075-y

Richter, T., Sens-Schönfelder, C., Kind, R., & Asch, G. (2014). Comprehensive observation and modeling of earthquake and temperature-related seismic velocity changes in northern Chile with passive image interferometry. *Journal of Geophysical Research: Solid Earth*, *119*(6), 4747–4765. https://doi.org/10.1002/2013jb010695

Sanders, C. O., Ponko, S. C., Nixon, L. D., & Schwartz, E. A. (1995). Seismological evidence for magmatic and hydrothermal structure in Long Valley caldera from local earthquake attenuation and velocity tomography. *Journal of Geophysical Research*, *100*(B5), 8311–8326. https://doi.org/10.1029/95jb00152

Schaefer, L. N., Kendrick, J. E., Oommen, T., Lavallée, Y., & Chigna, G. (2015). Geomechanical rock properties of a basaltic volcano. *Volcanology*, *3*, 29. https://doi.org/10.3389/feart.2015.00029

Scheu, B., Kern, H., Spieler, O., & Dingwell, D. B. (2006). Temperature dependence of elastic P- and S-wave velocities in porous Mt. Unzen dacite. *Journal of Volcanology and Geothermal Research*, *153*(1), 136–147. https://doi.org/10.1016/j.jvolgeores.2005.08.007

Schubnel, A., Benson, P. M., Thompson, B. D., Hazzard, J. F., & Young, R. P. (2006). Quantifying damage, saturation and anisotropy in cracked rocks by inverting elastic wave velocities. *Pure and Applied Geophysics*, *163*(5–6), 947–973. https://doi.org/10.1007/s00024-006-0061-y

Sens-Schönfelder, C., & Wegler, U. (2006). Passive image interferometry and seasonal variations of seismic velocities at Merapi Volcano, Indonesia. *Geophysical Research Letters*, *33*(21), 1–5. https://doi.org/10.1029/2006GL027797

Siratovich, P. A., Heap, M. J., Villenueve, M. C., Cole, J. W., & Reuschlé, T. (2014). Physical property relationships of the Rotokawa Andesite, a significant geothermal reservoir rock in the Taupo Volcanic Zone, New Zealand. *Geothermal Energy*, *2*(1), 10. https://doi.org/10.1186/s40517-014-0010-4

Siratovich, P. A., Sass, I., Homuth, S., & Bjornsson, A. (2011). Thermal stimulation of geothermal reservoirs and laboratory investigation of thermally-induced fractures. In *Proc., geothermal Resources council annual meeting* (pp. 1529–1535).

Siratovich, P. A., Villeneuve, M. C., Cole, J. W., Kennedy, B. M., & Bégué, F. (2015). Saturated heating and quenching of three crustal rocks and implications for thermal stimulation of permeability in geothermal reservoirs. *International Journal of Rock Mechanics and Mining Sciences*, *80*, 265–280. https://doi.org/10.1016/j.ijrmms.2015.09.023

Sparks, R. S. J., Bursik, M. I., Carey, S. N., Gilbert, J., Glaze, L. S., Sigurdsson, H., & Woods, A. W. (1997). *Volcanic plumes*. Wiley.

Stanchits, S., Vinciguerra, S., & Dresen, G. (2006). Ultrasonic velocities, acoustic emission characteristics and crack damage of basalt and granite. *Pure and Applied Geophysics*, *163*(5–6), 974–993. https://doi.org/10.1007/s00024-006-0059-5

Teklemariam, M., Beyene, K., AmdeBerhan, Y., & Gebregziabher, Z. (2000). Geothermal development in Ethiopia. In *Proceedings, world geothermal congress 2000* (pp. 475–480).

Thór Gudmundsson, B., & Arnórsson, S. (2002). Geochemical monitoring of the Krafla and Námafjall geothermal areas, N-Iceland. *Geothermics*, *31*(2), 195–243. https://doi.org/10.1016/S0375-6505(01)00022-0

Todd, T. P. (1973). *Effect of cracks on elastic properties of low porosity rocks*. Massachusetts Institute of Technology.

Tomac, I., & Sauter, M. (2018). A review on challenges in the assessment of geomechanical rock performance for deep geothermal reservoir development. *Renewable and Sustainable Energy Reviews*, *82*, 3972–3980. https://doi.org/10.1016/j.rser.2017.10.076

Varley, N., Connor, C. B., & Komorowski, J.-C. (2019). *Volcán de Colima: Portrait of a persistently hazardous volcano*. Springer.

Villaseñor, A., Benz, H. M., Filippi, L., De Luca, G., Scarpa, R., Patanè, G., & Vinciguerra, S. (1998). Three-dimensional P-wave velocity structure of Mt. Etna, Italy. *Geophysical Research Letters*, *25*(11), 1975–1978. https://doi.org/10.1029/98GL01240

Vinciguerra, S., Trovato, C., Meredith, P. G., & Benson, P. M. (2005). Relating seismic velocities, thermal cracking and permeability in Mt. Etna and Iceland basalts. *International Journal of Rock Mechanics and Mining Sciences*, *42*(7–8), 900–910. https://doi.org/10.1016/j.ijrmms.2005.05.022

Wang, H. F., Bonner, B. P., Carlson, S. R., Kowallis, B. J., & Heard, H. C. (1989). Thermal stress cracking in granite. *Journal of Geophysical Research*, *94*(B2), 1745–1758. https://doi.org/10.1029/JB094iB02p01745

Wang, X.-Q., Schubnel, A., Fortin, J., Guéguen, Y., & Ge, H.-K. (2013). Physical properties and brittle strength of thermally cracked granite under confinement. *Journal of Geophysical Research: Solid Earth*, *118*(12), 6099–6112. https://doi.org/10.1002/2013JB010340

Weaver, J., Eggertsson, G. H., Utley, J. E. P., Wallace, P. A., Lamur, A., Kendrick, J. E., et al. (2020). Thermal liability of hyaloclastite in the Krafla geothermal reservoir, Iceland: The impact of phyllosilicates on permeability and rock strength. https://doi.org/10.1155/2020/9057193

Yong, C., & Wang, C. (1980). Thermally induced acoustic emission in Westerly granite. *Geophysical Research Letters*, *7*(12), 1089–1092. https://doi.org/10.1029/gl007i012p01089

Zhang, F., Zhao, J., Hu, D., Skoczylas, F., & Shao, J. (2018). Laboratory investigation on physical and mechanical properties of granite after heating and water-cooling treatment. *Rock Mechanics and Rock Engineering*, *51*(3), 677–694. https://doi.org/10.1007/s00603-017-1350-8

Zhu, W., Baud, P., Vinciguerra, S., & Wong, T. (2016). Micromechanics of brittle faulting and cataclastic flow in Mount Etna basalt: Micromechanics of deformation in basalt. *Journal of Geophysical Research: Solid Earth*, *121*(6), 4268–4289. https://doi.org/10.1002/2016JB012826